UNIVERSITY OF CALIFORNIA,
IRVINE

# Functional Characterization of *in vitro* Models of Stem Cell-Derived Cardiomyocytes

DISSERTATION

submitted in partial satisfaction of the requirements
for the degree of

DOCTOR OF PHILOSOPHY

in Chemical and Biochemical Engineering

by

David Tran

Dissertation Committee:
Professor Steven C. George, Chair
Professor Nancy Da Silva
Professor Elliot L. Botvinick

2015

# DEDICATION

To my mother who has given me support and love all my life,

Nadine Thuy Tran.

# TABLE OF CONTENTS

Page

# LIST OF FIGURES

Page

# ACKNOWLEDGMENTS

For all the people who supported, challenged, and inspired me through my time at UCI, I must express my utmost gratitude:

To my graduate advisor, Dr. Steve George, for his patient mentoring and endlessly positive demeanor. I could always count on Steve for a weekly dose of inspiration and renewed focus, even in the face of adversity. For the countless lessons that have helped me mature as a scientist and aas a person while in the lab, I am truly grateful. To Dr. Elliot Botvinick and Dr. Nancy Da Silva for their continual support and encouragement as my dissertation committee.

To all the members of the George lab, whom I could not have asked any more of. Thank you to Dr. Claire Robertson who mentored me as a rotation student and PhD student. Claire was the first person to believe in my abilities and was always there to help. To Dr. Monica Moya who I worked very closely with throughout my studies. Monica's persistent dedication to performing high quality research has had a great impression on me. To Yosuke Kurokawa and Sandra Lam for their help. I will not forget how after moving to St. Louis and coming back to California on vacation, Sandra willingly and gladly came to UCI to help microfab extra device molds for my project. I truly believe Yosuke and Sandra have a bright future ahead of them. To Linda McCarthy for all her work running the ELCACT center, and all the life lessons she shared. And of course, to Dr. Luis Alonzo, whom I would consider my "brother". Luis was inspirational to me as a dedicated worker no matter the time of day, as a thoughtful researcher who I could bounce ideas with, as an overly positive person with infectious happiness, and as a genuine person who is generous to others.

To all of the other research labs that made this research possible and made my time at UCI enjoyable. Thank you to Dr. Mindy Simon and Dr. Abe Lee's lab for their expertise in microfluidic techniques and electrode fabrication. To Rupsa Datta, Dr. Michelle Digman, Dr. Enrico Gratton and the Laboratory for Fluorescence Dynamics for their help in FLIM microscopy and phasor analysis. To Ashley Fong and Dr. Chris Hughes' lab for their close collaboration with our lab. To Dr. Mo Mandegar and Dr. Bruce Conklin's lab for their generous gift of iPS cells and insight into cardiomyocyte research. To Dr. Himanshu Sharma, Eugene Lee and the rest of Dr. Michelle Khine's lab for their full support and endless supply of coffee that helped fuel the marathon that is graduate school. I am especially appreciative of Himanshu who is extremely helpful and selfless, as exemplified by the time he helped me attempt to fix the LSM for almost three hours amidst his own very busy day. To Dr. Marian Waterman and Dr. Harry Mangalam for their generosity and kindness.

To the International Foundation for Ethical Research for their financial support.

Finally, to Sophia Lin, for all her love and care. My appreciation is beyond words.

# CURRICULUM VITAE

**David Tran**

## Education

2015 Ph.D. in Chemical and Biochemical Engineering
University of California, Irvine

2011 M.S. in Chemical and Biochemical Engineering
University of California, Irvine

2009 B.S. in Chemical and Biomolecular Engineering
University of California, Angeles

## Experience

2010-2015 Graduate Student Researcher
University of California, Irvine
Advisor: Professor Steven C. George, MD, PhD

2008-2009 Undergraduate Student Researcher
University of California, Los Angeles
Advisor: Professor James C. Liao, PhD

2008 Manufacturing Engineering Intern
Baxter BioScience, Glendale

## Awards and Honors

2013-15 International Foundation for Ethical Research Graduate Fellowship

2012 Best Poster Award
IEEE-EMBS MNMC Conference

2012 Best Video Award
IEEE-EMBS MNMC Conference

2012 UC Irvine Student Research and Travel Grant

2011 HHMI-UCI Teaching Fellows Program

**PUBLICATIONS**

ML Moya#, **D Tran#,** and SC George. An integrated in vitro model of perfused tumor and cardiac tissue. *Stem Cell Res. & Therapy* 4 (Suppl 1):S15, 2013. #contributed equally as first authors on this manuscript.

CJ Robertson, **D Tran**, and SC George. Maturation phases of human pluripotent stem cell-derived cardiomyocytes. *Stem Cells* 31:829–837, 2013.

# ABSTRACT OF THE DISSERTATION

Functional Characterization of *in vitro* Models of Stem Cell-Derived Cardiomyocytes

By

David Tran

Doctor of Philosophy in Chemical and Biochemical Engineering

University of California, Irvine, 2015

Professor Steven C. George, Chair

Current preclinical methods to evaluate drug safety fail to accurately predict cardiotoxicity, the leading cause of drug withdrawal from the market. Human stem cell-derived cardiomyocytes represent an intriguing new source of cells for the development of *in vitro* drug screening platforms. However, questions of phenotypic immaturity, lack of analytical tools to monitor critical cardiomyocyte functions and simplicity of current cardiac tissue models, have delayed the acceptance of these new stem cell-based testing platforms. In this work, we surveyed the many aspects of the stem cell-derived cardiomyocyte phenotype and contrasted them to adult cardiomyocytes. Phasor fluorescent lifetime imaging microscopy (FLIM) analysis monitors metabolism of cells in a nondestructive and noninvasive manner. Phasor FLIM analysis was used to assess the transient metabolic signature of cardiac spheroids and to characterize the acute effect of cyanide poisoning on cardiomyocyte metabolism. Future cardiac drug testing platforms can be used in conjunction with phasor FLIM analysis to elucidate the metabolic effect of drugs. Finally, the effect of interstitial flow on a model of vascularized cardiac tissue was examined. Increased interstitial flow rates enhanced vascular network formation and

significantly increased cardiomyocyte growth in cardiac tissues. Methods to increase the complexity and maturity of cardiac tissue can potentially improve the predictive capability of stem cell-based drug testing platforms, and ultimately prevent unnecessary mortality by cardiac drug side effects.

CHAPTER 1

# Introduction

## 1.1 Prevalence and impact of heart disease

Advances in modern medicine, the greater prevalence of available nutrition, and improved sanitation in the past century have allowed humans to live much longer lives [4]. As previously common fatal diseases such as pneumonia, diarrhea and tuberculosis have been drastically reduced [5], the incidence of heart disease has continually risen. Deaths from heart disease have steadily risen from 137.4 deaths per 100,000 in the year 1900 to 362.0 per 100,000 in 1972. Since 1972, the death rate due to heart disease has slowly declined due to improved treatments and increased public prevention of cardiovascular risk factors such as smoking. Nevertheless, more than 83 million Americans [6] (~ 25% of the population) currently live with cardiovascular disease, further demonstrating a need for improved therapeutics for heart disease.

In an effort to reduce cardiac mortality rates, a large variety of medications have been developed to treat known risk factors such as high blood cholesterol, high blood pressure, and inflammation. High cholesterol levels correlate to a higher risk of cholesterol plaque buildup within the arteries, also known as atherosclerosis, which may rupture and cause stroke or myocardial infarction. The drug class of statins has been shown to block cholesterol formation within the liver, reducing the blood level concentration of cholesterol and effectively reducing the risk of a cardiovascular event by a third [7].

Another key regulator of atherosclerosis is the immune system. Plaque formation is initiated as monocytes and T cells infiltrate and accumulate within the arterial wall in

addition to cholesterol [8,9]. Statins also have additional beneficial effects of modulating the immune system and stabilizing plaques in order to prevent plaque rupture and stroke or heart attack [10]. High blood pressure, also known as hypertension, places additional stress on the heart, and is a known risk factor for myocardial infarction, heart failure, stroke and kidney disease [11]. Antihypertensive drugs include diuretics, angiotensin-converting-enzyme (ACE) inhibitors, angiotensin-receptor blockers (ARB), beta-blockers and calcium channel blockers.

Even with a large array of treatments available to treat heart disease at our disposal, there remains a great need for improved therapeutics that cost less. Treatment of heart disease places tremendous strain upon the economy. The cost of heart disease treatment in 2010 was approximately $200 billion dollars and is projected to rise to $918 billion in 2030 [6]. More effort must be placed towards finding new treatments that are cost efficient and have improved efficacy towards reducing the mortality of heart disease.

In order to discover safer and more effective cardioactive drugs, the FDA drug approval process may need to change [12]. The current drug developmental process from clinical testing to market approval takes on average 7.5 years [13] and costs between $500 million and $2 billion [14]. Before clinical trials on humans begin, preclinical testing of experimental drugs on animals is performed to determine preliminary ranges of safety and efficacy. Animal testing has the advantages of being multicellular, three dimensional, and possess multiple organs that allows for monitoring of off-target side effects, pharmacokinetics and pharmacodynamics testing. Unfortunately, animals are generally ill-suited for predicting drug safety and efficacy on human hearts. For example, drugs intended to treat heart disease [15,16] have been shown to be safe in animals, yet have unintended side effects in

humans, while other non-cardiac drugs that are safe in animals have toxic cardiac side effects in humans [17-22]. Our dependency on *in vivo* animal testing or *in vitro* animal cardiomyocytes, also known as heart cells, is due to the fact that human cardiomyocytes do not proliferate nor retain their phenotype when cultured *in vitro*. Improving the preclinical process could prevent potentially dangerous drugs from large-scale distribution to the public.

## 1.2 Promoting adolescence of iPS-derived cardiomyocytes

The recent development of human induced pluripotent stem (iPS) cell technology as a source for human cardiomyocytes provides exciting new opportunities for drug screening platforms that have the potential to replace preclinical animal testing. Human iPS cells were first derived from human fibroblasts in 2007 [23] and represent a renewable non-embryonic source of stem cells from adult humans without the ethical dilemma of embryonic stem cells. Human iPS cells are pluripotent, with the ability to differentiate into essentially any adult cell type. This includes adult cell types that, in general, do not divide or replicate, such as heart [24] and nerve [25] cells. As differentiation methods of human iPS cells into cardiomyocytes have improved [26,27], research has been focused towards preliminary use of human iPS-derived cardiomyocytes as a predictor of human drug response [28-31]. The advent of iPS cells has also opened the future of patient-specific drug testing platforms as iPS cells generated from a patient with a genetic disease retains the person's genetic material. For example, iPS cells derived from patients with long QT syndrome (LQTS) [32-36], catecholaminergic polymorphic ventricular tachycardia type 1 (CPVT1) [37] and hypertrophic cardiomyopathy [38] can be differentiated into cardiomyocytes

with the corresponding phenotypic characteristics of slow repolarization, mutated ryanodine receptor of the sarcoplasmic reticulum and enlarged morphology. Although human iPS cell technology has many advantages, more must be done to fully develop iPS technology to supplant animal testing. Human *in vitro* iPS testing is primarily unicellular and performed on a simple monolayer. These simple systems are conducive for rudimentary dose-response and mechanistic studies, but do not replicate the 3D *in vivo* environment.

Cardiomyocytes derived from human stem cells are phenotypically comparable to immature human cardiomyocytes, and may need to achieve a more mature state in order to accurately predict *in vivo* drug response. For example, adult cardiomyocytes are large and rectangular shaped (approximately 120 x 35 μm) [39] while human stem cell-derived cardiomyocytes are relatively small and oblong (15 x 10 μm) [40,41]. After time in culture (>35 days), stem-cell derived cardiomyocytes become more rectangular shaped (30 x 10 μm) [41] but still do not reach the size of adult cardiomyocytes, as shown in Figure 1.1. Human stem cell-derived cardiomyocytes also do not typically form a t-tubule network, necessary for excitation-contraction coupling in heart muscle cells [40]. Gene expression of iPS-derived cardiomyocytes resembles fetal cardiac tissue rather than adult cardiac tissue, specifically lacking in the expression of contractile proteins, ion channels and calcium handling proteins [42] . Consequently, action potential characteristics of iPS-derived cardiomyocytes are more immature when compared to an adult action potential, such as lower maximum diastolic potential [43], slow depolarization speed [24,43-45] and spontaneous beating [45-47]. With respect to metabolism, stem cell-derived cardiomyocytes have fewer

mitochondria [48], and therefore rely on glycolytic metabolism rather than oxidative phosphorylation [28].

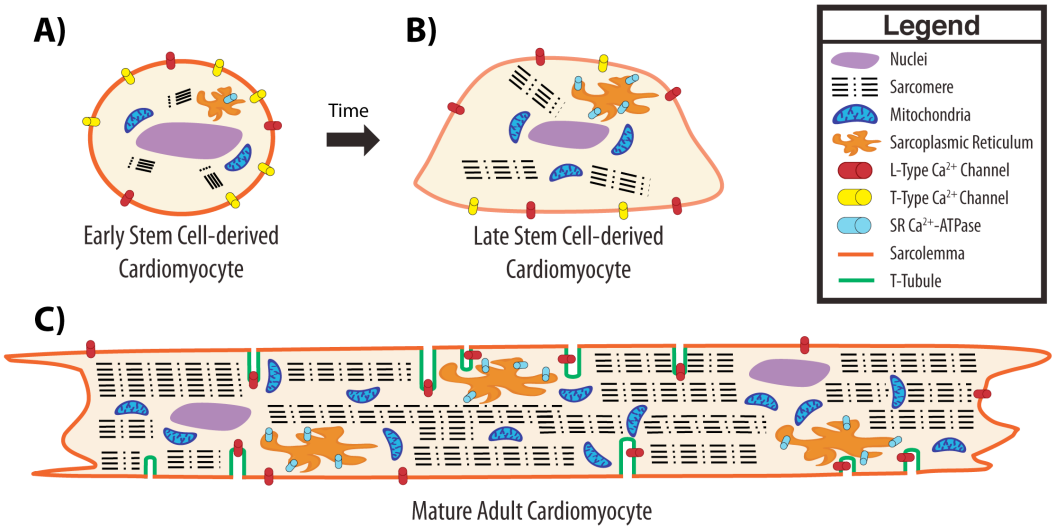


**Figure 1.1 Phenotypic comparison of stem cell-derived cardiomyocyte to mature adult cardiomyocyte.** Stem cell-derived cardiomyocytes are initially small and oblong-shaped (A) and become more rectangular (B) after time in culture. In contrast, mature adult cardiomyocytes (C) are much larger, may be multinuclear, contain more mitochondria, and develop organized sarcomeres. T-tubule formation and l-type calcium channel expression permit mature electrophysiological phenotype. Reprinted by permission from John Wiley and Sons: Stem Cells [2], copyright 2013.

In an attempt to induce maturation of stem cell-derived cardiomyocytes, researchers have taken inspiration from normal cardiac development [49] to mimic key components of the native cardiac microenvironment. Maintenance of cardiomyocytes typically consists of two-dimensional cell culture on rigid polystyrene, which fails to recapitulate the native microenvironment and may not be conducive towards cardiac maturation. Furthermore, transfer of primary adult heart cells to tissue culture plastic immediately induces dedifferentiation characterized by loss of sarcomeric structure [50].

Similar to *in vivo* cardiomyocytes, cardiomyocyte maturation *in vitro* can be stimulated simply by time in culture. Stem cell-derived cardiomyocytes continually cultured elongate from an oblong shape into a rectangle morphology (>35 days) [46,51], upregulate hypertrophic-related genes (>60 days) [46], multinucleate (>80 days) [52], exhibit mature

action potentials (>110 days) [52,53], develop myofibrillar Z, A, H and I-bands (>180 days) [54] and finally M-bands (>360 days) [54]. These studies illustrate the ability of stem cell-derived cardiomyocytes to mature into adult-like heart cells, but they achieve maturation much more slowly in comparison to the human embryo cardiac development (full heart formation within 50 days [55]). In order to accelerate maturation, more complex methods of cell culture may be necessary.

A pacemaker region, also known as the sinoatrial (SA) node, macroscopically controls heart muscle contraction. The SA node initiates an action potential and transmits the signal through the rest of the heart via purkinje fibers [56] to coordinate heart contractions in a concerted manner. Previous research has shown the importance of excitation-contraction coupling upon natural development of heart tissue [57]. In contrast, stem cell-derived cardiomyocytes differentiated *in vitro* spontaneously beat without external stimulation. Application of electrical stimulation to stem cell-derived cardiac tissues leads to myofibril organization, increased conduction velocity and improved ion handling [58,59]. Interestingly, an applied pacing regimen at a superphysiological rate (6 Hz) further improves cardiac phenotype.

The heart is composed of multiple cell types, each with specific roles necessary for normal heart function. Non-cardiomyocyte cell types present within the heart include endothelial cells, smooth muscle cells, nerve cells, and cardiac fibroblasts [60]. Although research has been focused towards differentiating stem cells into cardiomyocytes at high purity levels, non-cardiomyocyte cells may be necessary for cardiomyocyte maturation [61]. For example, human stem cell-derived cardiomyocytes isolated from a fully differentiated population exhibit stunted electrophysiological development compared to cardiomyocytes

left in coculture [43]. Coculture with endothelial cells so far has not shown induction of hypertrophy, but rather stimulates cardiomyocyte proliferation [62]. Additional studies are needed to further understand the role of non-cardiomyocyte cells upon the maturation of cardiomyocytes.

The heart is a dynamic organ, continually pumping nutrients throughout the body. In contrast, static two-dimensional culture does not appropriately model the dynamic in vivo environment of the heart muscle. Recapitulating the dynamic microenvironment is important as cells contain mechanosensing transduction pathways that react to stress, strain and stiffness [63]. Optimization of substrate stiffness for transmission of work can modulate the ability of cardiomyocytes to beat and develop striated myofibrils [64]. Platforms that cyclically stretch cells in vitro attempt to capture the dynamic strain profile of the heart and demonstrate accelerated phenotypic maturation. Within 72 hours of cyclical mechanical stimulation, human stem cell-derived cardiomyocytes hypertrophy by elongating, and increase expression of cardiac contractile proteins [46,62,65,66]. Mechanical stretching also induces the expression of cardiac ion channel proteins [62], corresponding to faster calcium handling function [66].

In addition to mechanical cues, the native cardiac extracellular matrix contains a rich mixture of proteins, glycoproteins and proteoglycans [67] that may support specific cellular responses. These include collagen type I, III, IV, V, VI, elastin, fibrinogen, fibulin, laminin, lumican and perlecan. Fibronectin is a key component of matrigel that induces efficient differentiation of stem cells into cardiomyocytes [26]. Additionally, a combination of fibronectin and laminin can increase cardiac lineage specification by upregulation of corresponding integrin expression and subsequent activation of transduction pathways

responsible for differentiation [68]. Decellularized cardiac extracellular matrix is an intriguing option for mimicking the native microenvironment as it retains many features of the extracellular composition of the native heart matrix [67]. Encapsulation of embryoid bodies within cardiac extracellular matrix improves cardiac differentiation of the embryoid bodies, organization of sarcomeres, and cardiac gene expression [69]. In fact, cardiac extracellular matrix alone is a stronger modulator of cardiomyocyte differentiation than growth factors or small molecules traditionally used to induce differentiation. Although these results are promising, further research should evaluate the use of cardiac matrix encapsulation for phenotypic maturation.

## 1.3 Microfluidic platforms for drug screening

Microfluidic technology has advanced tremendously over the past two decades with the advent of soft lithography [70], and stands to revolutionize current methods of drug screening. This methodology allows for easier fabrication of microchannels with rapid prototyping capability. Most importantly, the primary material used for soft lithography, polydimethylsiloxane (PDMS), is cheap, biocompatible and suitable for cell culture. Less reagents and cells are required as processes are miniaturized using microfluidics, thus reduces overall cost [71]. Miniaturization also leads to a higher density of processes and increases spatial efficiency necessary for industry-level high-throughput screening.

A primary advantage of microfluidics is the ability to recreate complex processes in a simple manner. The spatial resolution of soft lithography permits tissues to be formed into specific geometries depending on the application. Channels can be patterned to form gradients [72] of chemical or biochemical molecules necessary for cell signaling [73-75].

Spatiotemporal cues such as paracrine factors are important in altering the biological responses of cells. Simple changes in channel design can control pressure, shear stress, interstitial flow and residence time [76]. In addition to channels, other features able to be fabricated include valves [77-79], mixers [80-83], reactors [84,85] and separators [86]. These tools allow miniaturization of complex processes such as electrophoresis, chromatography, binding assays, patch clamp, low signal detection, RNA extraction and DNA synthesis [87].

An increasing amount of *in vitro* microfluidic models are being created for drug efficacy and toxicity screening [88]. These new models may replace current *in vitro* testing methods, which are typically simple monolayers, and do not accurately replicate *in vivo* tissue. This is important as the success of *in vitro* models is based on how well they mimic the human body's response. Controlling gradients of chemical and biochemical cues has been shown to positively influence cell phenotype [74]. Microfluidic channels are designed for physiological delivery of nutrients and removal of metabolites and waste. Proper fluid flow has been shown to promote growth of tissues within a microfluidic device [89,90]. Devices can also be designed to match physiological residence time of drugs delivered to tissue. Recreating physiological residence times permits the study of pharmacodynamics *in vitro* [91,92], which is typically studied only in animals. In combination with well-designed fluid mechanics, microfluidic chips can support the culture of three-dimensional tissues, which respond and function very differently than typical two-dimensional models [93-98].

Microfluidic technology allows for precise control in tissue engineering applications. Although microfluidics can control interstitial flow to promote functionalization of microvasculature in tissue [90,99], further control features may be necessary to develop more complex tissues. For example, cardiomyocyte tissue grown within a microfluidic device

may benefit from electric field stimulation. Electrical stimulation has been shown to mature both mechanical contraction force [100] and electrophysiology of stem cell-derived cardiomyocytes [58,101]. Currently, the most common technique to pace 3-dimensional cardiac tissue cultured within microfluidic devices has been to insert large platinum [101] or carbon [100] rods into the device to serve as electrodes. Physically inserting rods into a fluidic device may work for large devices but may not be feasible or precise when scaling down to microfluidic dimensions. Another method to control electrical field within microfluidic devices has been the use of low melting solders into surrounding fluidic chambers [102]. Although the use of solder electrodes is simple and easy to use, solder electrodes must be enclosed as typical low melting point solders are toxic to cells. Electrical resistivity of PDMS is relatively large and therefore the electrical input of an enclosed solder electrode correspondingly requires very large input voltages in order to pace nearby cardiomyocyte cells. Such a pacing system requires expensive electrical equipment and is potentially dangerous when handled. Future research will need to focus on recreating additional facets of *in vivo* tissue, such as electrical pacing, into *in vitro* testing platforms to better model *in vivo* response.

## 1.4 Fluorescent lifetime imaging for metabolic analysis

PDMS microfluidic devices are optically clear, and are thus amendable to optical-based assays to probe cellular phenotype and response [103-105]. Fluorescent lifetime imaging microscopy (FLIM) is based on the length of time a fluorescent molecule is excited before returning to its ground state [1]. A laser scans the sample on a pixel-by-pixel basis while photomultiplier tubes (PMTs) record fluorescence intensity over time. A fluorescence emission is shaped, as shown in Figure 1.2, to the following exponential decay equation:

$$I(t) = I_0 e^{-\frac{t}{\tau}} \tag{1.4.1}$$

where I(t) is the intensity with respect to time, $I_0$ is the initial intensity, t is time and τ is the lifetime. The emission lifetime can be described as:

$$I(\tau) = \frac{I_0}{e} \tag{1.4.2}$$

In order to quantify lifetime of an emission, FLIM measurements are recorded using two modalities: time domain and the frequency domain.

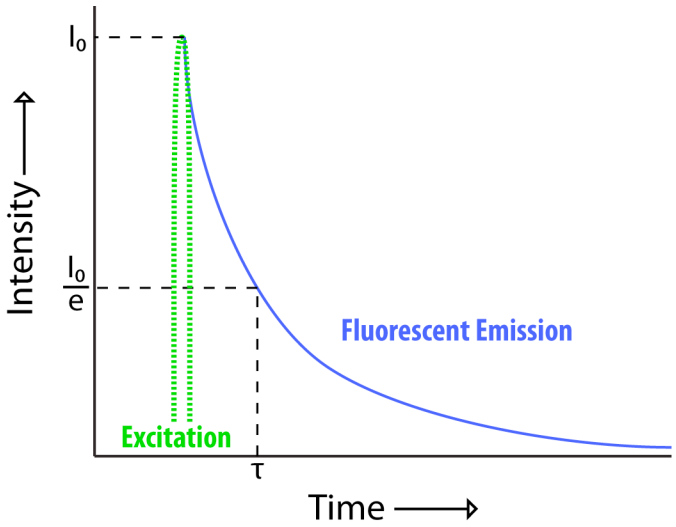


**Figure 1.2 Characteristic fluorescent emission as described in Equation 1.4.1.** An excitation pulse (green) excites the fluorescent molecule to $I_0$ and then decays over time (blue). The lifetime of the emission, τ, is described as the time for the intensity to reduce to $I_0/e$.

For the time domain method, a very short excitation is pulsed at the sample and the subsequent emission is recorded using a photo multiplier tube (PMT). The PMT can only measure photons at a specific time and therefore many scans of each pixel must be taken to recreate the intensity decay of the emission signal. Although this method is relatively straight forward, there are several drawbacks. Acquiring enough photons to reconstruct each emission signal is relatively slow. If the pixel contains multiple species of fluorophores, fitting a decay profile with multiple exponential functions is computationally difficult, and requires multiple iterations to solve. The long time period for computation is also compounded by the total amount of pixels to be fitted.

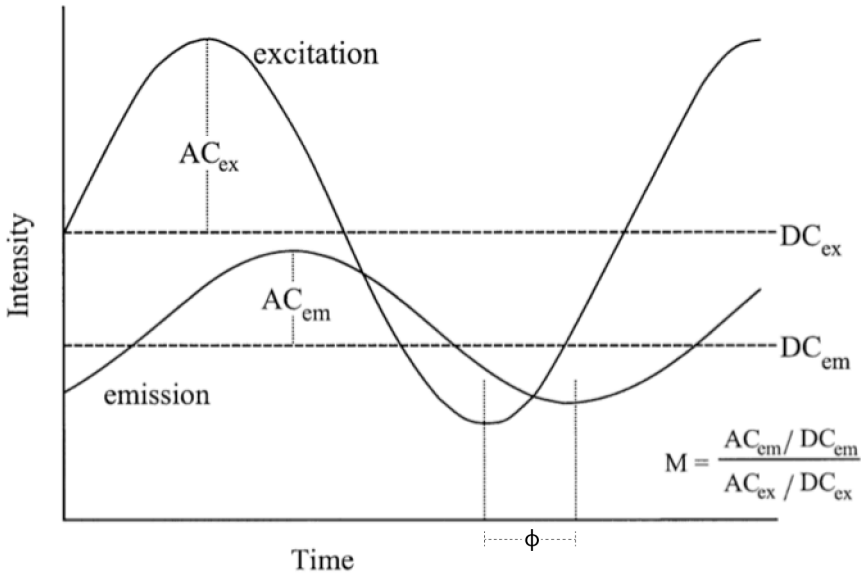


**Figure 1.3 Fluorescence emission in the frequency domain.** The fluorophore is excited using a sinusoidal light source and results in a sinusoidal emission. The fluorescence emission oscillates at the same frequency as the excitation, but with an altered amplitude and shifted phase. Reprinted and adapted with permission from Elselvier: Methods in Cell Biology [1], copyright 2003.

In comparison, the frequency domain utilizes a sinusoidal excitation source. As shown in Figure 1.3, the resulting emission is also sinusoidal but with a modulated amplitude, *M*, and shifted phase, ϕ. Rather than laboriously fitting exponentials to recorded emissions,

analysis of the frequency domain method simply converts decay emissions into a phasor plot, as shown in Figure 1.4. A phase vector can be described as a vector defined by M and ϕ, with the corresponding x and y coordinates:

$$g = M * \cos(\Phi) \tag{1.4.3}$$

$$s = M * \sin(\Phi) \tag{1.4.4}$$

Each fluorescent species has a distinct representation along the phasor plot, allowing for quick analysis.

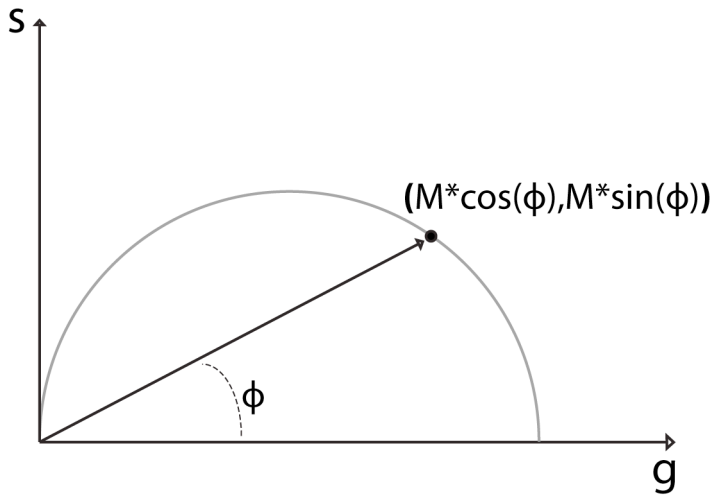


**Figure 1.4 Example phase vector in phasor plot.** A phasor is defined by the emission's modulation, M, and its phase shift, ϕ.

Features of cellular metabolism can be analyzed using phasor plot analysis of FLIM due to the autofluorescence of endogenous NADH molecules. Under two-photon excitation at 740 nm, NADH autofluoresces and emits light between 400 and 500 nm. Interestingly, the emission lifetime of NADH varies greatly depending on whether the NADH species is bound to protein (3.4 nsec) or free (0.4 nsec). Application of phasor plot analysis, as shown in Figure 1.5, can therefore be used to determine the ratio of free NADH to bound NADH. This

technique can be used to assay whether cells shift their metabolism in favor of free or bound NADH in reaction to stimuli [106].

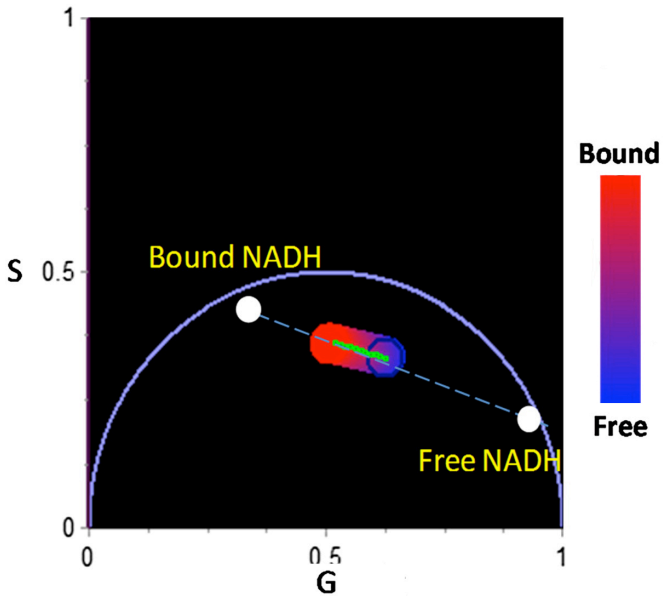


**Figure 1.5 Phasor position of bound NADH and free NADH.** Bound NADH and free NADH have characteristically different lifetime emissions and therefore reside in different areas of the phasor plot (white circles). Depending on the ratio of bound to free NADH species, the phasor vector will lie along the dotted line. Samples with higher bound to free NADH will be indicated further left on the line (red) while samples with more free NADH will be to the right of the line (blue). Reprinted and adapted with permission from Elsevier: Biophysical Journal [3], copyright 2012.

The primary method of metabolism for proliferating cells is glycolysis [107], which supports the generation of biomass but inefficiently generates ATP. A byproduct of glycolysis is the formation free-floating NADH within the cytoplasm. In contrast, mature cells primarily utilize oxidative phosphorylation to efficiently create ATP. Oxidative phosphorylation occurs primarily within the mitochondria. NADH participates in the electron transport chain process by binding to the transmembrane protein NADH dehydrogenase, and is thus protein-bound. By analyzing shifts in the ratio of free to bound NADH present within the cell, we can infer changes in metabolism within the cell.

The following chapters aim to further develop the reliability and predictive capabilities of *in vitro* stem cell-derived cardiomyocyte drug testing platforms to replace the use preclinical animal testing. Stem cell-derived cardiomyocytes represent a powerful new source of cells for the development of new *in vitro* drug screening platforms, but immediate adoption of this technology is hampered by questions of phenotypic immaturity, lack of analytical tools to monitor critical cardiomyocyte functions and simplicity of current cardiac tissue models. This dissertation begins by surveying the many aspects of stem cell-derived cardiomyocyte phenotype and contrast them to adult cardiomyocytes. We use phasor FLIM analysis to demonstrate a new tool for the assessment of cardiomyocyte metabolism and characterization of the metabolic effects of drugs. We then explore the effects of interstitial flow on a model of vascularized cardiac tissue with respect to vessel network formation and cardiomyocyte function. Tools that better characterize cardiomyocyte response and methods to increase the complexity and maturity of cardiac tissue can potentially improve the capability of stem cell-based drug testing platforms, and ultimately prevent unnecessary mortality by cardiac drug side effects.

# CHAPTER 2

# Maturation phases of human pluripotent stem cell-derived cardiomyocytes

## 2.1 Abstract

Human pluripotent stem cell derived cardiomyocytes (hPS-CM) may offer a number of advantages over previous cardiac models, however questions of their immaturity complicate their adoption as a new in vitro model. hPS-CM differ from adult cardiomyocytes with respect to structure, proliferation, metabolism and electrophysiology, better approximating fetal cardiomyocytes. Time in culture appears to significantly impact phenotype, leading to what can be referred to as early and late hPS-CM. This work surveys the phenotype of hPS-CM, including structure, bioenergetics, sensitivity to damage, gene expression, and electrophysiology, including action potential, ion channels, and intracellular calcium stores, while contrasting fetal and adult cardiomyocytes with hPS-CM at early and late time points after onset of differentiation.

## 2.2 Introduction

There is an urgent need for novel cardiomyocyte models: ischemic heart disease remains the number one killer in the western world [108], congenital cardiomyopathies affect 1-2% of live births [109,110], and drug-induced cardiotoxicity is a leading cause of market withdrawal [111]. Human pluripotent stem cell-derived cardiomyocytes (hPS-CM) may offer significant advances in the study of cardiac disease and treatments [112,113]. Similar to currently available cardiomyocyte models, hPS-CM contract rhythmically [51] and respond appropriately to numerous cardioactive drugs [112,114]. In addition, hPS-CM can also be

manipulated genetically[115], maintained in *in vitro* culture long term (1+ yrs.) [116], and be created from adult patients with genetic conditions (in the case of cardiomyocytes sourced from induced pluripotent stem cells, hiPS-CM) [117-120], and may engraft into damaged hearts *in vivo* [121-123].

Given the potential of these cells, and the excitement surrounding them (>2000 publications since the first report a decade ago [124]), it is timely to address the similarity of these cells to adult human cardiomyocytes, and how they might be used as models of such. Open questions surrounding these cells include: How do we best assess cardiomyocyte maturity? How well do hPS-CM model embryonic or adult CM *in vitro*? How does maturity change during in vitro culture? When can hPS-CM be used as models for adult CM?

It is frequently noted that hPS-CM resemble human fetal cardiomyocytes [51]; however, no previous review has systematically quantified the similarities. This is complicated by high variation in phenotype between hPS-CM studies, partially explained by differences in cell line of origin and culture conditions. Furthermore, evidence suggests that hPS-CM develop a more mature, adult-like phenotype with time in culture, yet differences between early and late phase hPS-CM have not yet been described. Therefore, this review will define "early" and "late" phase hPS-CM phenotype, and describe how hPS-CM resemble embryonic and adult cardiomyocytes with respect to key markers of maturity, including ultrastructure, metabolism, gene expression and electrophysiology.

## 2.3 hPS-CM structure and function resemble embryonic cardiomyocytes

### 2.3.1 Definition of early and late phase hPS-CM

In this work, hPS-CM will be defined as spontaneously contractile cells derived from a human pluripotent cell line, to the exclusion of contractile cells derived from adult mesenchymal stem cells [125-128] or from mouse pluripotent stem cells, which have been described elsewhere [129-131]. Recent reviews have covered methods to create [123,132-135] and purify hPS-CM [136], as well as their electrophysiology [137], drug response [112,114], and function after transplant in vivo [122,138]. Cardiomyocytes derived from hiPS (hiPS-CM) and human embryonic stem (hES-CM) cells appear to be relatively similar, but will be compared when data describing differences is available.

hPS-CM vary in maturity, thus, we will define hPS-CM as either early phase, defined as contractile cells, with some proliferative capacity and with embryonic like electrophysiology (i.e. small negative membrane potential and small action potential amplitude), or late phase, defined by loss of proliferative capacity and more adult-like electrophysiology. hPS-CM show early phase characteristics for generally the first month after initiation of contraction, with development of late phase characteristics arising afterwards. Different elements of maturity appear to be affected by line [24,31,139], time in culture [24,140], co-cultured cells [141] and culture conditions [142,143]; however, the factors affecting maturity remain largely unknown. This suggests that after initiation of contraction genetic and environmental factors interact leading to a more mature phenotype; however, the process is incompletely understood.

### 2.3.2 Morphology

It has been widely reported that hPS-CM structurally resemble embryonic or fetal cardiomyocytes [144,145]. However, potentially important differences are seen when these cells are compared to embryonic or adult cardiomyocytes. Adult cardiomyocytes are large and cylindrical (approximately 150 x 10 μm for ventricular cells) [146], while embryonic and fetal cardiomyocytes are smaller [147]. Similarly, early hPS-CM (initiation of contraction- 21 days) are small and round to slightly oblong, approximately 5-10 μm in diameter [51,139,148] (Fig. 1). Late hPS-CM (>35 days) develop a more oblong morphology (30 μm x10 μm), similar to the dimensions of human embryonic cardiomyocytes, but remain small compared to adult [51]. In addition, most adult cardiomyocytes are bi- or multi-nucleated, whereas hPS-CM are mono-nuclear, similar to early embryonic cardiomyocytes [147].

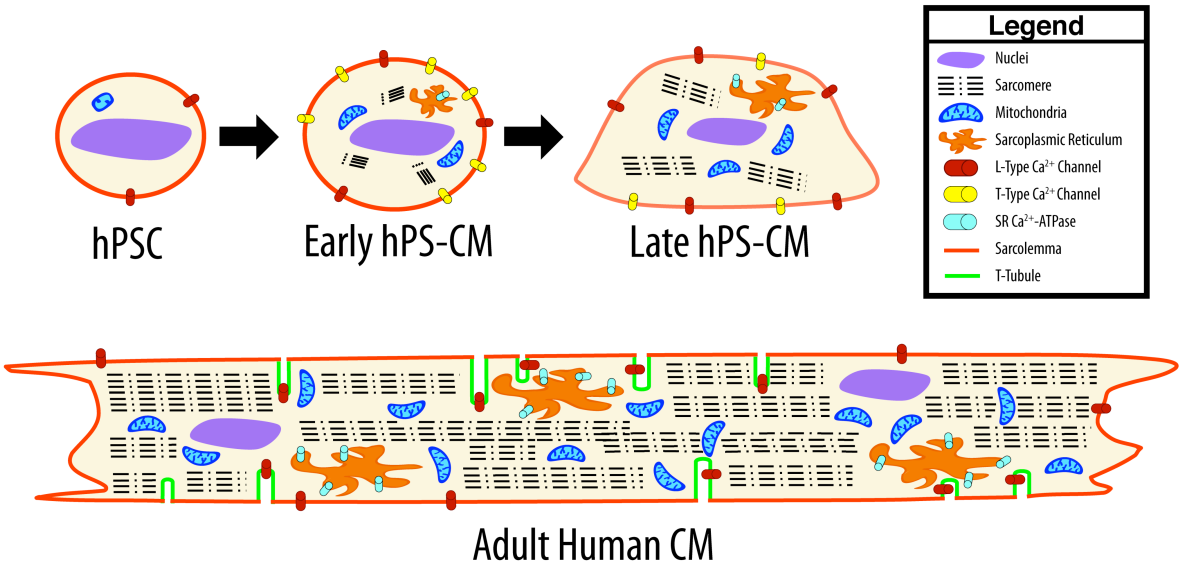


**Figure 2.1 A visual comparison of early hPS-CM, late hPS-CM, and adult CM**. Characteristics of early and late phase hPS-CM depend strongly on time in culture since the initiation of contraction (early- proliferative, late- nonproliferative). Note that late hPS-CM differ from early hPS-CM with respect to shape, sarcomeric area and receptor expression. Adult CM are far larger, with multiple nuclei, large sarcomeric area, and large numbers of mitochondria.

The extensive t-tubule network present in adult ventricular cardiomyocytes is absent in both hPS-CM and embryonic cardiomyocytes [146]. As a result, excitation-contraction coupling is slower, and calcium primarily enters the cell through the sarcolemma instead of releasing from the sarcoplasmic reticulum [149-152]. Thus, early hPS-CM structurally resemble embryonic cardiomyocytes. With increasing time in culture, late hPS-CM develop a more adult-like morphology, but do not appear to develop t-tubules or multi-nucleation as shown in Figure 2.1.

### 2.3.3 Function: Proliferation

Early hPS-CM proliferate [51,143,153], similar to embryonic or fetal mammalian cardiomyocytes [154-156]. In contrast, adult cardiomyocytes are amongst the most slowly dividing cell types [157]. Over time in culture, proliferative capacity of hPS-CM decreases from that of stem cells (24-48 hr doubling time [158]) to low levels: at four weeks, only 10% cells were BrdU+ after a 24 hr incorporation assay [143] and no Ki-67$^{+}$ cells were observed [51], similar to changes seen in fetal cardiac development[154] (Fig. 2). Atrial natriuretic factor (involved in cardiomyocyte proliferation [159,160]) is expressed in hPS-CM [161,162]. In summary, early hPS-CM proliferate at a lower rate than their pluripotent progenitors whereas late hPS-CM can be considered non-proliferating cells.

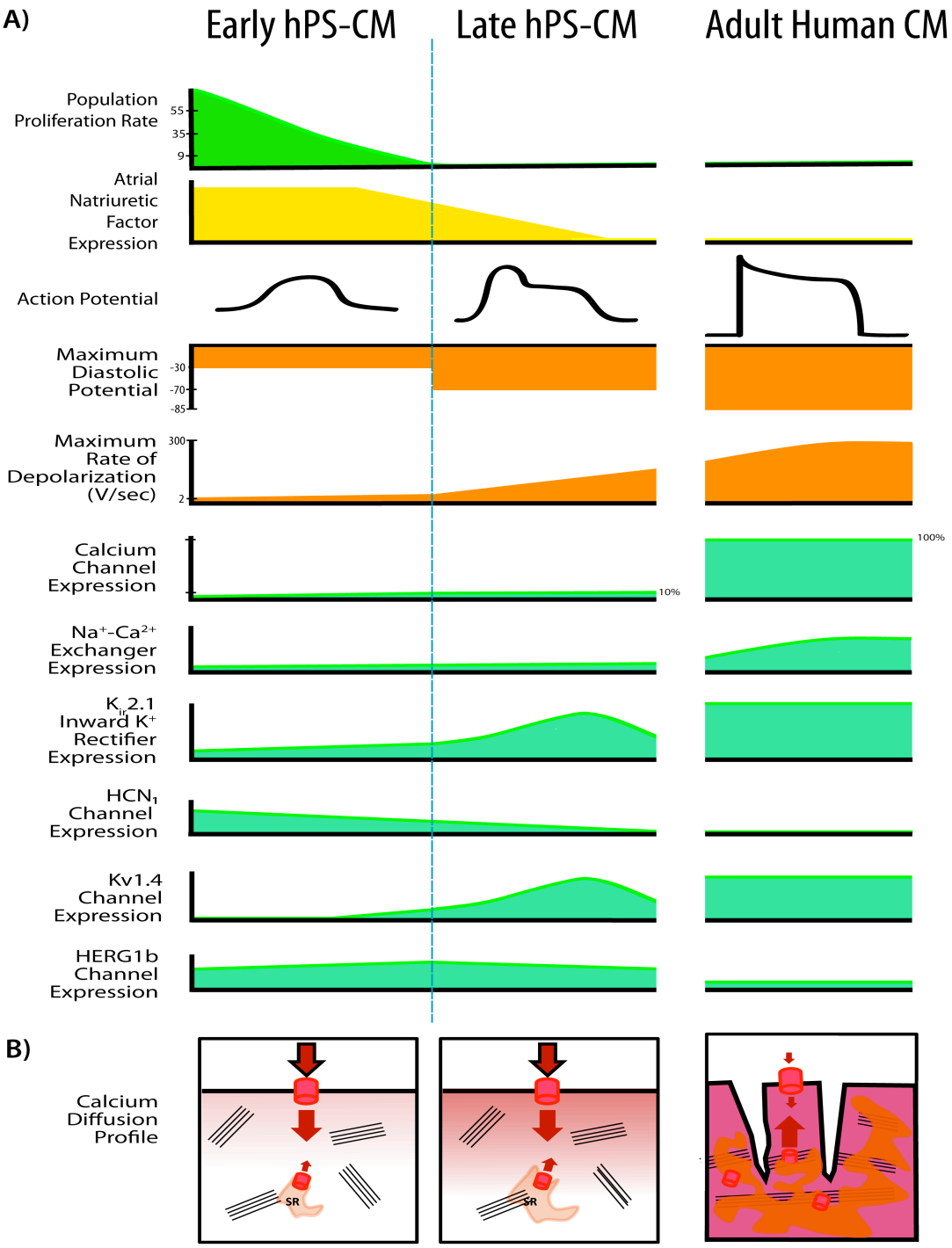


**Figure 2.2 Comparison of cardiomyocyte phenotype.** a) An overview of major changes seen with increasing time in culture. Large changes in action potential characteristics (orange) are seen with time in culture, as well as expression of key ion channels (teal). Panel B shows calcium influx profiles for early and late hPS-CM compared with adult CM. Note that in early hPS-CM, almost no calcium is released from the sarcoplasmic reticulum, leading to slow, diffusion-limited calcium influx. Late hPS-CM perform better, but still show slow influx compared to adult.

### 2.3.4 Function: Gene expression

The transcriptional profile of hPS-CM is starkly different from their originating pluripotent stem cells. Important differences include loss of pluripotency transcription factors and upregulation of mesodermal and cardiac markers [163-166]. Once differentiated, hPS-CM display a relatively homogeneous, cardiac-like gene expression program. Interestingly, gene expression of hiPS-CM and hES-CM is surprisingly similar, with only 1.9% of genes differentially expressed in these two cell types, despite dramatic differences between expression profiles in the undifferentiated hiPS and hES sources [167].

hPS-CM expression of contractile genes was not discernibly different from fetal heart tissue (20 week gestation) in one study of enriched early hPS-CM(age unknown) [163]. Global gene expression profile of purified early hPS-CM is more similar to fetal cardiac tissue (age unspecified) than to adult cardiac tissue; however hPS-CM gene expression clustered more closely with either fetal or adult cardiac tissue than with pluripotent stem cells [42]. Bigger differences are seen when comparing hPS-CM and adult heart tissue, with important differences seen in a number of cardiac ion channel and calcium handling genes, once again highlighting the immature phenotype of hPS-CM [165,168].

### 2.3.5 Function: Metabolism and bioenergetics

Contractile machinery and mitochondria fill two-thirds of the cytoplasmic volume in adult CM (myofibril cell area- 40% [169] to 52% [170] and mitochondria- 15% [169] to 25% [48,170]). In contrast, hPS-CM [136] and embryonic CM [171] both show smaller sarcomeric regions [172,173], and have more moderate numbers of mitochondria [48] (Fig. 1). Similarly, expression of

contractile and cytoskeletal genes is much lower in hPS-CM (unknown age) compared to fetal (20 week) or adult cardiomyocytes [163].[42].

Adult cardiomyocytes are highly metabolically active and depend on oxidative metabolism for synthesis of ATP (fatty acid oxidation accounts for 90% of acetyl-CoA production [174,175]). In comparison, embryonic and fetal cardiomyocytes rely on glycolysis for production of ATP [171,176] (fatty acid oxidation<15% of acetyl-CoA production [177]) resulting in a relatively hypoxia resistant phenotype and providing substrates for protein production [171]. hPS-CM showed primarily glycolytic metabolism in one study (in late, nonproliferative hPS-CM) which evaluated oxygen consumption rates [178], and mixed glycolytic and oxidative metabolism in another which assessed incorporation of radiolabeled carbon into metabolites (age unknown) [48]. hPS-CM are also able to metabolize lactate, unlike hPS [48]. Higher expression of oxidative phosphorylation genes and proteins are seen in hPS-CM compared to pluripotent stem cells, suggesting that these cells have the potential to use this metabolic pathway [48,179,180], though the expression level lags behind fetal tissue [163]. It remains unclear whether time in culture can alter hPS-CM preferred energy substrate.

### 2.3.6 Sensitivity to Damage and Apoptosis

It is unclear to what extent *in vitro* adult cardiomyocytes mimic the *in vivo* response to noxious stimuli. *In vivo*, adult cardiomyocytes may survive an entire lifetime (>80 yrs.), while *in vitro* adult cardiomyocytes rarely survive more than a few days [181]. In stark contrast, hPS-CM are already culture-adapted, with reports of cells maintaining viability and contractility for a year [116,182]. These observations clearly complicate comparisons of

the sensitivity to damaging insults of hPS-CM with both *in vivo* and *in vitro* adult CM, and additional work is required to fully understand the differences in apoptotic cascades between these conditions.

Despite these limitations, some evidence suggests that hiPS-CM respond similarly to stimuli that cause damage to adult cardiomyocytes. For example, cardiotoxic tyrosine kinase inhibitors such as sunitinib and sorafenib demonstrate arrhythmogenicity and increased apoptosis in hiPS-CM at clinically cardiotoxic doses of the drug [178,183]. Likewise, doxorubicin, a cardiotoxic chemotherapeutic which is believed to act through oxidative stress [184], can induce apoptosis in hiPS-CM [185], as well as microtubule derangement [186]. Similarly, direct application of oxidizers such as hydrogen peroxide, induce apoptotic responses in hPS-CM [187,188]. This process is mediated by opening of the mitochondrial permeability transition pore, and could be prevented with anesthetic mediated preconditioning [187,188], thus recapitulating the behavior seen in adult cardiomyocytes [189].

Embryonic human cardiomyocytes are resistant to hypoxia [190], whereas adult cardiomyocytes are highly dependent on an adequate oxygen supply [191]. As both hPS-CM and embryonic cardiomyocytes are predominantly glycolytic [178], it may be inferred that hPS-CM would likewise be resistant to hypoxia. However, the sensitivity of hPS-CM to ischemic stimuli has not been fully established. In summary, despite differences in metabolism, hPS-CM are sensitive to oxidative stress and cardiotoxic agents at levels expected from clinical use; however, their sensitivity to ischemia has not been characterized.

### 2.3.7 Cardiac-specific inotropic and chronotropic receptors

Several key chronotropic responses are observed in hPS-CM and may be affected by time in culture. α, β1, and β2 adrenoceptor response have all been demonstrated in hPS-CM [192,193]. A positive response to isoprenaline (β receptor agonist) challenge is almost universally performed in studies of hPS-CM [24,31,124,172,192-201], suggesting that all hPS-CM have some β-receptor expression, regardless of cell line of origin, differentiation method. As *in vivo*, isoprenaline increases contraction rate (positive chonotropy), increases the amplitude of the calcium transient and decreases the relaxation time [193]. Unlike adult cardiomyocytes, however, isoprenaline does not increase contraction force [201], once again demonstrating the immaturity of this cell type. β2 response accounts for 17-37% [193] of the total response to isoprenaline, akin to fetal cardiomyocytes. With increased time in culture, hPS-CM demonstrated increased chronotropic β agonist response [193,200]. In summary, β adrenoceptor response is present in hPS-CM, and shares characteristics with fetal cardiomyocytes, and may be amplified with time in *in vitro* culture.

Several studies have demonstrated a chronotropic response to carbacholine [192,194,195], thus showing muscarinic receptor activity. Finally, increased intracellular cAMP increases contraction rate in hPS-CM via the phosphodiesterase inhibitor IBMX [124,172], and the adenylyl cyclase activator forskolin [172,192]. It is unclear whether *in vitro* maturation time affects the magnitude of these responses, or whether these responses affect force of hPS-CM contraction.

### 2.3.8 Electrophysiology: Spontaneous beating rate

Spontaneous and synchronous contraction is seen as early as 5 days after the initiation of differentiation [202], and can be maintained for over one year in culture [116] (in stark contrast to adult CM [181]). Different basal rhythms have been reported, ranging from 21 [196] to 52 beats per minute (BPM) [193], with most reporting ~ 40 BPM [24,195,203]. The rate of contraction may be affected by cell line, cultures conditions, time since differentiation, and time since the onset of contraction. hiPS-CM from iPS from patients with long QT syndrome show slower repolarization, thus recapitulating the *in vivo* phenotype [117,118,204-206].

Time in culture affects beating rate, though magnitude and direction of this change appears to vary with study. Several studies have reported moderate increases in contraction rate (30 to 75 BPM at 70 days [193] and 40 to 85 BPM at 60 days [24]) though a decrease has also been reported (45 to 5 BPM over the course of 63 days [195]). hES-CM show faster and stronger rhythms than hiPS-CM [24], which may be due to earlier initiation of contraction or the differences between hiPS and hES cells [167,207]. In summary, spontaneous beating is the principal hallmark of differentiated hPS-CM, and beating rate is affected by line of origin and by time in culture.

### 2.3.9 Electrical Properties: Action potential

hPS-CM contract spontaneously and synchronously, as noted previously, and are thus electrically active. Cells displaying atrial-, nodal-, and ventricular-like APs have been reported [208-210]. In addition, hPS-CM action potential characteristics vary between studies and within studies with different cell lines [24], differentiation methods [211], and time in

culture [141]. Variation in a single population of hPS-CM has also been demonstrated, suggesting that even using the same cells, methods, and at the same time point, the electrophysiological characteristics of hiPS-CM are more heterogeneous than those in an adult heart [211]. hPS-CM from the same EB (a more homogeneous environment) showed greater homogeneity in action potential duration than hPS-CM from same population but different EBs [24], highlighting the potential important role of a common extracellular environment in hPS-CM maturation.

Most reported action potential characteristics are less mature than adult cardiomyocytes: maximum diastolic potential (MDP) for adult ventricular myocytes is -85mV [212] whereas early hPS-CM MDP is approximately -30mV [141] which improves to -60 to -75mV in late hPS-CM [24,205,213-216]. The maximum rate of depolarization ($dv/dt_{max}$ or $V_{max}$) in adult cardiomyocytes is extremely fast, ranging from 300 V/sec in healthy hearts [212] to about 100V/sec in heart failure [217]. In contrast, early hPS-CM show extremely slow depolarization depolarization speeds. Early hPS-CM depolarize at 2V/sec [141], improving in late hPS-CM to 10 to 40 V/sec [24,205,215,216] (with 2 studies reporting 130-150 V/sec [211,218] - Fig. 2). Similar parameters for embryonic or fetal cardiomyocytes are not available.

### 2.3.10 Electrical Properties: Ion channels

The major ionic currents normally present in adult cardiomyocytes are expressed in hPS-CM, though frequently at abnormal levels (Fig. 2). The calcium channels are necessary for contractility, as is NCX [219,220] and HCN [213]. In early hPS-CM, sodium channel inhibition does not prevent spontaneous contraction, but in late hPS-CM the same inhibition blocked spontaneous contraction [141].

The potassium currents considered to be responsible for arrhythmias are expressed in hPS-CM [118,205,221] (Fig. 2). As a result, considerable interest in using hPS-CM for anti-arrhythmic drug screening exists and has been reviewed [31,114,204,222]. Some arrhythmias in hPS-CM are affected by time in culture, and thus may be a measure of *in vitro* maturity [211,223].

### 2.3.11 Electrical Properties: Intracellular calcium

The extent of the sarcoplasmic reticulum (SR) and its necessity for automaticity in hPS-CM is a matter of debate. In adult cardiomyocytes, calcium induced calcium release (CICR) from the SR contributes almost 70% of the total calcium release [224]. In contrast, hPS-CM, which have very little SR function in the early phase [150,225-229], demonstrate calcium transients that are smaller and slower [230], with most cation influx is through the cell membrane [228,231]. This results in abnormal diffusion of calcium into the cell [226], and reduces the synchrony in contraction necessary for large force generation [201]. (Fig. 2B)

Reports vary as to the presence and function of the SR, possibly due to changes with maturity [149-151,225,228]. However there is consensus that intracellular calcium stores are smaller than in adult cardiomyocytes [225,232]. Calcium handling and response to compounds that modify calcium handling (e.g., nifedipine, ryanodine) appear to vary significantly between lines [226,233], and between embryonic and induced pluripotent derived CM [226,234], including larger intracellular calcium stores, though line to line differences dominate differences between hES and hiPS class [24]. Over time in culture, increased sarcoplasmic reticulum function is seen as assessed by caffeine-induced calcium release [225].

When paced, adult cardiomyocytes show a positive force-frequency relationship; that is, at faster pacing rates, greater calcium transients and force of contraction are seen [224]. This relationship requires both significant intracellular calcium stores and electrical coordination across the cell (the t-tubule network again ensures that the entire cell depolarizes rapidly and homogeneously [224]). In contrast, hPS-CM have consistently shown negative force-frequency relationships [149,200,232]. In these cells, calcium primarily enters the cell across the cell membrane and diffuses though the cytoplasm, a slower process [235]. Similarly, post-rest potentiation (i.e., an increased uptake in calcium in resting cardiomyocytes after rapid pacing) is not seen [149], or seen only to a low extent [200] in hPS-CM. It has not been studied whether these properties improve with time in culture, but the increased sarcoplasmic reticulum function seen in late hPS-CM suggests they may be more adult-like.

Some evidence suggests that non-SR calcium stores play a key role in excitation-contraction coupling in hPS-CM [150]. IP3 receptor (IP3R) is expressed, and co-localizes with sarcomeres and the cell nucleus [225,228], suggesting it may play a role in release of non-SR calcium stores. In adult cardiomyocytes, IP3R appears to regulate non-contractile calcium signaling only [236-238], although abnormal IP3R expression can cause arrhythmia [236]. In hPS-CM, IP3R may be involved in contractility as contraction rate is sensitive to IP3 and IP3R antagonists [225,228]; however, this observation may depend on inhibition of ryanodine receptors (RYRs) [141].

### 2.3.12 Structural and functional sarcoplasmic reticulum proteins

The structural and functional proteins in the SR show low and varied expression as would be expected from the evidence provided earlier on the underdeveloped SR in hPS-CM. Expression of the ryanodine receptor (RYR) is noted in a number of studies [141,239], though at only a small fraction (0.1%) of the adult level [225]. Most reports state that application of ryanodine slows spontaneous contraction rate [120,146,200,225,228,231,240,241], though two studies saw no such change [226,229]. Similarly, one study reports close physical association between RYRs and L-type calcium channels [231], which would allow for efficient CICR [231], though other studies reported no such association [146,239]. It should be noted that the co-localization of these two proteins in adult cardiomyocytes is debated [242]. SERCA, the sarcoplasmic reticulum $Ca^{2+}$ ATPase pump, is also expressed in hPS-CM [226,243] at levels similar to fetal cardiomyocytes [239], but a variable response to its inhibitor thaspargin has been reported [149,228].

Not surprisingly, proteins known to regulate SR function are also abnormally expressed in hPS-CM. Calsequestrin, which binds calcium and allows for dense packing of the ion in the SR, is absent in a number of studies [149,150,227,239] though present in one [200]. Interestingly, transgenic calsequestrin overexpression was enough to improve calcium handling and SR maturity in hiPS-CM [227]. Phospholamban, an endogenous inhibitor of SERCA, is absent in some studies [149,150], though present in others [243], and its presence is inferred from a positive drug response [193]. Some of this variability may be due to variable (widely unreported) hPS-CM age or manual selection of spontaneously beating cells, as more rapidly beating cells may have less phospholamban expression (*in vivo* phospholamban is

known to repress cardiac contractility) [244,245]. Junctin and triadin, which potentiate RYR [246], were expressed at low levels in one study [226], and absent in another [239].

## 2.4 Conclusions

hPS-CM are a heterogeneous population of cells that recapitulate some features of embryonic and adult cardiomyocytes. hPS-CM contract spontaneously and synchronously, express numerous cardiac specific genes and proteins, and recapitulate several important electrophysiological features of adult cardiomyocytes. Recapitulation of fetal or adult cardiomyocyte phenotype may require novel culture methods better recapitulating the *in vivo* niche. Furthermore, time in culture, specifically time since the onset of differentiation or time since spontaneous contraction, is a major factor affecting proliferation, structure, intracellular calcium stores, and ion channel expression. It is unclear why time in culture should have such profound effects on hPS-CM phenotype, though several studies have emphasized the importance of paracrine signaling and cellular milieu in maturation, suggesting better recapitulation of the cardiac cellular niche will improve maturity. Nonetheless, it is convenient to define early and late phase hPS-CM based on phenotypic markers that include sarcomeric organization, sarcoplasmic reticulum, and membrane ion channels that impact such integrated behaviors as cell proliferation and the action potential. Despite limitations, hPS-CM demonstrate significant potential as a tool to enhance basic biological understanding, improve *in vitro* drug screening, and thus create new therapeutic options. Remaining challenges include improving the magnitude and consistency of intracellular calcium stores, improving sarcomeric volume and organization, creating consistent reproducible cell populations, and determining the mechanisms of

increased maturity with time in culture.

# CHAPTER 3

# Transient metabolic and functional effects of extracellular matrix on human stem cell-derived cardiomyocytes

## 3.1 Abstract

Metabolism of stem cell-derived cardiomyocytes is critical to their function, yet a simple, rapid, and nondestructive method to characterize cardiomyocyte metabolism is not currently available. Here we describe the contractility, calcium handling and metabolism of human induced pluripotent stem cell-derived cardiomyocyte spheroids encapsulated within extracellular matrix (ECM). ECM composed of cardiac-derived ECM (cECM) or collagen reduced spontaneous beating rate and increased calcium transient duration. Phasor fluorescent lifetime imaging microscopy (FLIM) analysis demonstrates that cardiomyocyte metabolism shifts to a more glycolytic state, rather than oxidative phosphorylation, over a period of 8 days, irrespective of matrix composition. FLIM analysis characterized the acute effect of cyanide poisoning, which significantly decreased long lifetime pixels from 72.69% to 40.13% percent of total pixels in 30 minutes of exposure. We conclude that Phasor FLIM analysis can be applied to future cardiac drug testing platforms to elucidate metabolic effects of drugs.

## 3.2 Introduction

Accurately predicting adverse cardiac side effects of new pharmaceutical drugs is difficult, and currently relies heavily on animal testing. This dependency on *in vivo* animal testing or *in vitro* animal cardiomyocytes is due to the fact that primary human cardiomyocytes do not proliferate nor retain their phenotype when cultured *in vitro*. Although animal models allow insight into pharmacokinetics and whole organ drug response, some drugs have been shown to only effect cardiomyocytes of human origin [247]. Several dangerous cardiotoxic drugs have subsequently failed during costly large human clinical trials (e.g. BMS-986094) [248] or after FDA approval (e.g., Vioxx) [249]. Indeed, unwanted cardiac side effects are one of the top reasons for drug market withdrawal.

The advancement of human induced pluripotent stem (iPS) cell technology provides exciting new opportunities for drug screening platforms that may replace animal testing. Development of human iPS-derived cardiomyocytes (iPS-CM) as a viable research and therapeutic tool has been accelerated by recent reports describing more efficient cardiac differentiation in defined conditions [26,27] as well as the ability to differentiate into specific cardiomyocyte lineages including ventricular [250], atrial [251], and nodal [252] cells. This technology could simultaneously improve the success rate of drugs passing human clinical trials, while reducing the use of animals in research. Human iPS-CM offer many advantages over animal models, including human origin, culture adaptation, and ability to create patient-specific lines for inherited disorders such as long QT syndrome [253,254]. Nonetheless, in order to fully replace animal testing for cardiac safety, human iPS drug screening platforms should be 3D tissues rather than simple monocultures to better recapitulate heart tissue.

Various tissue engineering methods have been used to create 3D cardiac tissues, including self aggregation of iPS-CM into scaffold-free 3D spheroids. Cardiac spheroids, also known as cardiospheres, can be generated reproducibly on a large scale and the aggregation process enhances the purity of the cardiomyocyte population to 80-100% [255]. To demonstrate applicability of cardiac spheroids as an *in vitro* cardiac model, cardiac spheroids responded normally when subjected to external electrical, pharmacological and physical stimuli [256]. Although human cardiac spheroid response to stimuli has been characterized well with regards to contractile function and protein expression, analysis of hiPS-CM spheroid metabolic response to external stimuli has yet to be described.

Metabolic phenotype is inextricably connected to cardiomyocyte function. Cardiomyocyte cells contain relatively large amounts of mitochondria (~35% volume [257] vs. ~5% volume in skeletal muscle [258]) in order to handle the perpetually large energy demand necessary to support continuous cyclical contraction. Abnormal metabolic function results in reduced cardiac contractile function [259] and ultimately may lead to heart failure [257]. Typical methods to characterize *in vitro* metabolism require cell culture as a monolayer [260], provide indirect measurements via gene expression [261-263], utilize radioactive isotopes [260], or require cellular lysis [264]. Phasor fluorescent lifetime imaging microscopy (FLIM) represents a label-free, nondestructive method to derive a metabolic signature of live cells and tissues by measuring the endogenous intracellular fluorophore nicotinamide adenine dinucleotide (NADH) [265-268]. NADH is present within the cell in either a free or protein-bound state, distinguishable by FLIM as either a short or long fluorescent lifetime, respectively. Free NADH is generally a byproduct of glycolysis, while protein-bound NADH primarily occurs in the electron transport chain of the mitochondria. Phasor

analysis of FLIM can quickly discern the ratio of free:bound NADH on a pixel by pixel basis [269]. Therefore, FLIM has the potential to measure transient metabolic changes or metabolic responses to a wide range of stimuli.

In this study, we encapsulated 3D human iPS-CM spheroids within extracellular matrix, and characterized contractile function, calcium handling and metabolism as a function of time. Metabolism was assessed using non-destructive fluorescent lifetime imaging (FLIM) phasor plot analysis [266]. We conclude that iPS-CM spheroids encapsulated within extracellular matrix shift towards a more glycolytic phenotype over time and cardiac extracellular matrix both reduces spontaneous beating rate and increases calcium transient duration.

## 3.3 Methods

*Human iPS-derived Cardiomyocyte Spheroid Generation*

Wild-type human iPS cells (WTC-11 [270,271]) were provided as a gift from Dr. Bruce Conklin at the Gladstone Institute of Cardiovascular Disease, San Francisco. The WTC-11 iPS line was derived from a healthy male volunteer with a normal electrocardiodiagram and no known family history of cardiac disease [272]. For non-invasive calcium indication, the WTC-11 iPS line was genetically encoded with the ultrasensitive calcium protein sensor, GCaMP6f [273], through transcription activator-like effector nuclease (TALEN)-mediated genome editing [274]. The GcAMP6f protein consists of green fluorescent protein (GFP), the calcium-binding protein calmodulin (CaM), and the CaM-interacting M13 peptide. Calcium binding to the CaM-13 complex causes a conformational change in the protein complex, which increases the fluorescent intensity of the GFP. The fast green fluorescent indicator

GCaMP6f under control of the constitutively expressed CAG promoter, and puromycin antibiotic resistance gene under control of the endogenous promoter, were encoded into the AAVS1 locus of the WTC-11 iPS genome. Human iPS cells containing the GCaMP6f cassette were subsequently selected by puromycin (0.5 μg/mL).

Differentiation of iPS cells into cardiomyocytes was performed using a small molecule-based Wnt modulating protocol [27]. Briefly, iPS cells were maintained with mTeSR1 (STEMCELL Technologies) in 6-well plates coated with Matrigel (BD Biosciences). At 80% confluence, iPS cells were dissociated with Accutase (Invitrogen) for 4 minutes at 37°C and plated (Day -4) onto 12-well plates coated with matrigel at a density of 33,000 cells/cm$^2$ in mTeSR1 with 10 μM Y-27632 (Tocris). The medium was replaced every 24 hours for 3 days (Day -3 to Day -1) with mTeSR1 only. On Day 0, differentiation of cells was initiated by canonical WNT activator 12 μM CHIR99021 (Selleck Chemicals) in RPMI 1640 medium supplemented with HEPES (Life Technologies) and B27 supplement without insulin (Life Technologies). After 24 hours (Day 1), media was replaced with RPMI 1640 with B27 minus insulin only. On Day 3, cells were treated with Wnt inhibitor 5 μM IWP-2 (Tocris) in a 50:50 blend of conditioned media and fresh RPMI 1640 with B27 minus insulin. On Day 5, the media was replenished with RPMI 1640 with B27 minus insulin only. On Day 7 and every 2-3 days, the media was changed with RPMI 1640 with B27 with insulin.

Beating cardiomyocytes (20-45 days old) were dissociated into single cells using 200 U/mL collagenase in Hank's balanced salt solution (Life Technologies) for 1 hour and then 0.25% trypsin/EDTA (Life Technologies) for 5 minutes at 37°C. Cells were then resuspended and seeded into AggreWell 400 (STEMCELL Technologies) plates at 720,000

cells per well. Cardiomyocyte spheroids were allowed to aggregate, and then self-assembled for two days before encapsulation within extracellular matrix.

*Decellularization of Cardiac Extracellular Matrix (cECM)*

Myocardial matrix was derived from porcine hearts using previously published protocols [1, 2]. Hearts were harvested from pigs immediately after euthanasia. The atria and right ventricle were removed from the heart and the remaining left ventricle cut into pieces (~2 mm in thickness). The tissue was briefly rinsed with deionized water followed by 1% (wt/vol) sodium dodecyl sulfate (SDS) in phosphate buffered saline (PBS) for 4 days. Lastly, tissue pieces were stirred overnight in deionized water to remove SDS. After decellularization, ECM pieces were lyophilized and milled with a Wiley Mini Mill (Thomas Scientific) to create a powder. To generate the hydrogel, pepsin (Sigma) was dissolved in 0.1 N HCl at 1 mg/mL and added to the myocardial matrix powder at 10 mg/mL. After 48 hours of constant stirring, the partially digested liquid matrix was brought to pH 7.4 using sodium hydroxide (NaOH) and 10x PBS. Neutralized matrix was then aliquoted, lyophilized, and stored at -80C for later use.

*Hydrogel Encapsulation of Human iPS-CM Spheroids*

Cardiomyocyte spheroids were suspended in different ratios of extracellular matrix. The combinations of extracellular matrix included 10 mg/mL bovine fibrinogen (Sigma-Aldrich) dissolved in Dulbecco's phosphate buffered saline (DPBS, Life Technologies), 9 mg/mL rat tail collagen (BD Biosciences), and 10 mg/mL cardiac extracellular matrix. All matrices denoted as a partial percentage had the remaining volume completed with fibrin.

Varying volumes of 50U/mL thrombin was used corresponding to the percentage of fibrinogen mixed within the ECM mixture. Spheroids resuspended in ECM mixture were then pipetted into a glass bottom dish (World Precision Instruments) with three polydimethylsiloxane (PDMS, Dow Corning) retention rings attached, each with a diameter of 8mm and an approximate height of 1 mm. The tissues were incubated for 30 minutes at 37°C to allow full polymerization and then fed RPMI 1640 supplemented with B27 with insulin. The media was collected and replaced every 2 days.

*Intracellular Calcium Imaging and Analysis*

Calcium transients of cardiomyocyte spheroids were analyzed by visually recording fluorescent activity of GCaMP6 during spheroid contractions. Videos were taken at 15.65 Hz using MetaMorph software (Molecular Devices) with an Olympus IX83 inverted microscope (Olympus) connected to a black and white CCD digital camera (Hamamatsu). Videos were saved as a TIFF stack and imported into ImageJ (NIH). A ROI was applied over each frame of the video to measure the average intensity. The data was imported into MATLAB (MathWorks). An automated script identified the start and peak of each contraction, then applied an n-th order (n=2-10) polynomial fit to normalize the decay of signal due to photobleaching. The script then calculated beating rate, calcium transient duration 90% (CTD90) and calcium transient amplitude. CTD90 was defined as the duration of time that the calcium transient exceeds 10% of the maximum or peak intensity depolarization and repolarization. Calcium transient amplitude was defined as the difference between basal fluorescence intensity during relaxation and maximum calcium intensity during contraction.

*FLIM and Phasor Analysis*

FLIM was performed on a Zeiss LSM 710 microscope (Carl Zeiss). A tunable titanium:sapphire Mai Tai laser (Spectra-Physics) was used for 2-photon NADH excitation at 740nm. Image scan speed was 25.21 µs/pixel at an image size of 256 × 256 pixels. For separation of excitation from emission signal, a dichroic at 690 nm was employed. Photons were detected by a Hamamatsu H7422P-40 photomultiplier tube with a bandpass emission filter of 460/80 nm. FLIM data was acquired using an A320 FastFLIM FLIMbox (ISS). For acquisition and FLIM data processing, SimFCS software developed at the Laboratory of

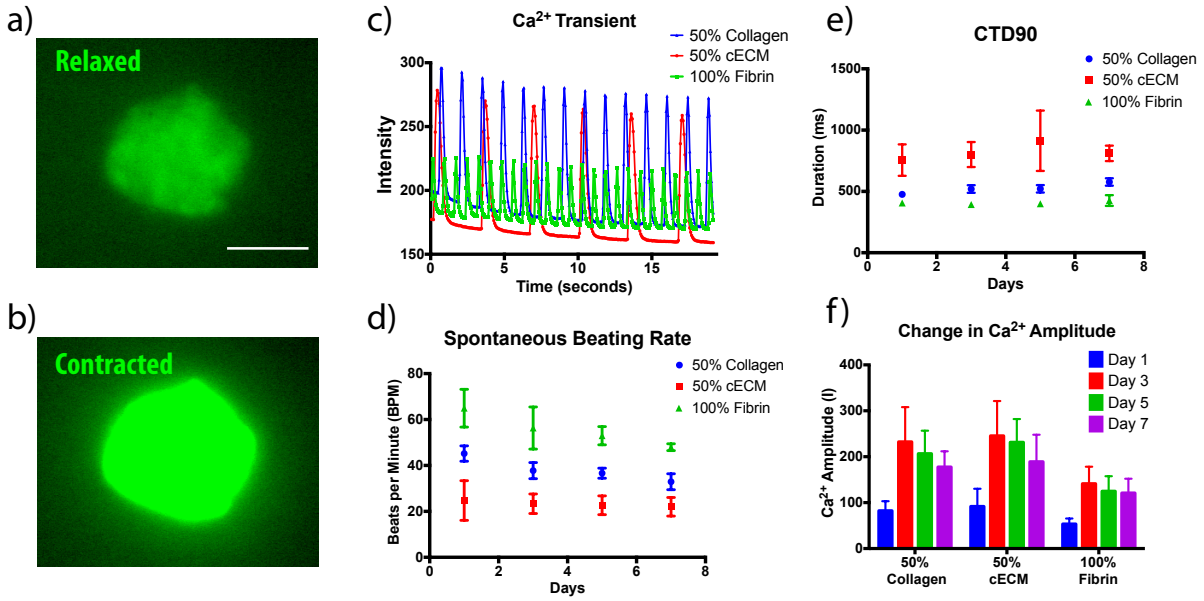


*Figure 3.1:* Characterization of GCaMP6-reported $Ca^{2+}$ Function within human iPS-CM spheroids. Representative image of cardiac spheroid at a (a) relaxed state and (b) contracted state (scale bar = 50 µm). c) Representative calcium transient intensity plot of cardiac spheroids within different matrix compositions. d) Spontaneous beating rate significantly decreased with respect to time in culture (two-way ANOVA, P <0.0001) and matrix composition (two-way ANOVA, P <0.0001). e) Calcium transient duration (CTD90) of cardiac spheroids was significantly effected by matrix composition (two-way ANOVA, P<0.0001). f) Calcium amplitude, indicative of the difference between the relaxed and contracted state, grew in magnitude from Day 1 to Day 3, and then subsequently leveled off or decreased.

Fluorescence Dynamics (LFD) was used. Fluorescent lifetime images were calibrated with Rhodamine 110.

For analysis of fluorescence lifetime data, a phasor transformation approach was employed [269]. As a fit-free method, the lifetime decay of each pixel within the image was converted into a point in the phasor plot by applying phasor transformation as has been described previously [265].

*Statistical significance*

Student's t-test and one-way ANOVA was performed where a p-value < 0.05 was considered significant. The data are expressed as mean ± standard deviation.

## 3.4 Results

We characterized human iPS-CM spheroid function once they were embedded into various extracellular matrices. Beating rate and calcium handling were measured by recording videos of the green fluorescent calcium indicator protein GCaMP6 genetically encoded into the iPS cells. The iPS-CM spheroids have low basal fluorescence when relaxed (Fig. 3.1a) and fluoresce bright green when contracted (Fig. 3.1b). Fluorescent intensities were plotted as a function of time to characterize beating rate and calcium handling (Fig. 3.1c). Matrix composition significantly reduced spontaneous beating rate, where spheroids in matrix composed of collagen or cECM beat at a markedly slower rate than in fibrin (two-way ANOVA, P <0.0001, Fig. 3.1d). With time in culture, cardiac spheroids exhibited reduced contraction rates (two-way ANOVA, P <0.0001). Calcium transient duration (CTD90) was markedly longer with more variability when spheroids were encapsulated in

cECM (two-way ANOVA, P <0.0001, Fig. 3.1d). Cardiac spheroids in all conditions began beating with a relatively small calcium transient amplitude, defined as the max intensity subtracted by basal intensity, which then increased by Day 3 and subsequently decreased over time (Fig. 3.1e).

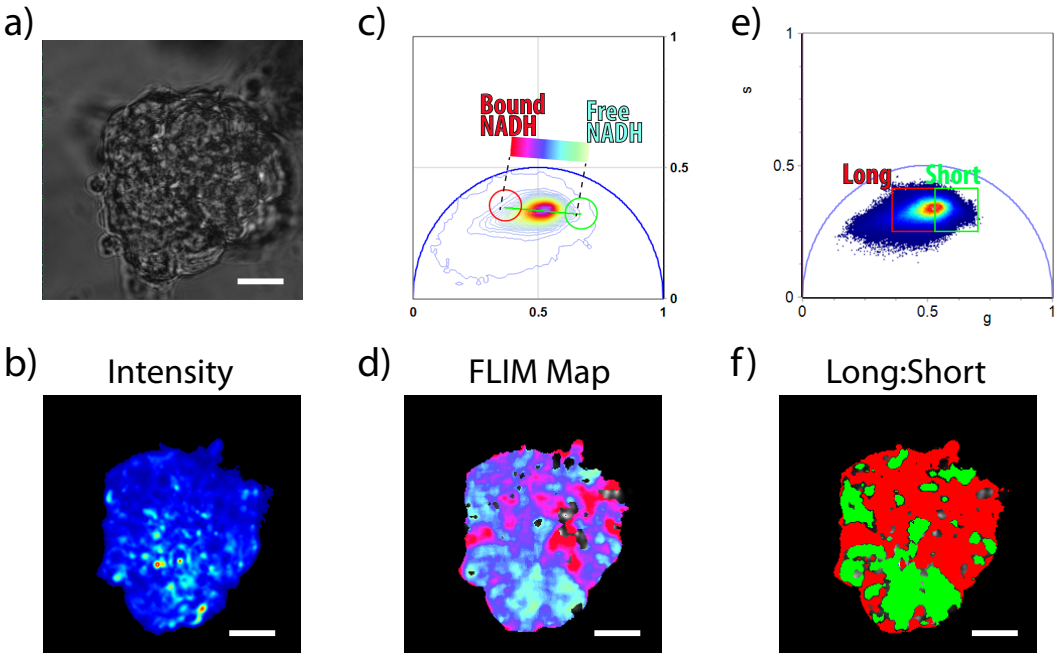


*Figure 3.2:* Phasor FLIM analysis of cardiomyocyte spheroid metabolism. a) Bright field image of human iPS-CM spheroid b) Two-photon fluorescent intensity image of endogenous NADH excited at 740 nm. c) Phasor histogram of FLIM image of cardiac spheroid. A linear color scheme (red to cyan-white) corresponds to relative concentrations of free NADH to bound NADH. d) NADH FLIM map of cardiac spheroid. e) Division of FLIM pixels into long and short lifetime groups for quantification. f) Corresponding FLIM map with long and short lifetime. (scale bar = 25 μm)

We performed label free FLIM imaging of endogenous autofluorescent NADH on human iPS-CM spheroids encapsulated in extracellular matrix (Fig. 3.2a). Figure 2b depicts a representative two-photon fluorescent intensity profile of a cardiac spheroid excited at 740 nm. The entire image was subject to phasor transformation on a pixel by pixel basis as previously described [266]. Depending on the ratio of free to bound NADH present, a pixel will be transformed into different positions along the phasor plot (Fig. 3.2c). The pattern of the

metabolic signature within the phasor plot represents a distribution of different ratios of free and protein-bound NADH. The pixels are colored based on their relative composition of free:bound NADH and then mapped spatially onto the FLIM image to indicate areas of predominantly free NADH (cyan) and areas of primarily bound NADH (red) (Fig. 3.2d). For quantification, we divided all pixels into two groups with half of the pixels designated as a long lifetime and the other half as short lifetime for quantification (Fig. 3.2e,f).

We measured transient metabolic changes of human iPS-CM spheroids by performing time-lapse FLIM of NADH. After encapsulation, the metabolism of cardiac spheroids shifted over a period of seven days towards a more glycolytic phenotype with higher free/bound NADH ratios (Fig. 3a). Encapsulation of cardiac spheroids within different extracellular matrix compositions did little to effect the metabolic signature and did not reverse the shift towards a more glycolytic state. Over time in culture, cardiac spheroids demonstrated a decrease in long lifetime pixels at a rate of -7.78% ± 1.53% of pixels/day and significantly decreased from 84.94% ± 11.50% of total pixels on Day 1 to 28.61% ± 15.91% on Day 8 (t-test, $P<0.0001$; Fig. 3.3b).

Human iPS-CM spheroids were exposed to potassium cyanide (KCN), a known inhibitor of cellular respiration. Interference of cellular respiration by potassium cyanide shifts the FLIM phasor distribution by increasing the free/bound NADH ratio indicated by the phasor FLIM color map (Fig. 3.4a). Exposure to KCN (4mM) for 30 minutes altered the metabolic signature quickly by decreasing the long lifetime pixels from 72.69% to 40.13% percent of total pixels (t-test, $P<0.01$, Fig. 3.4b).

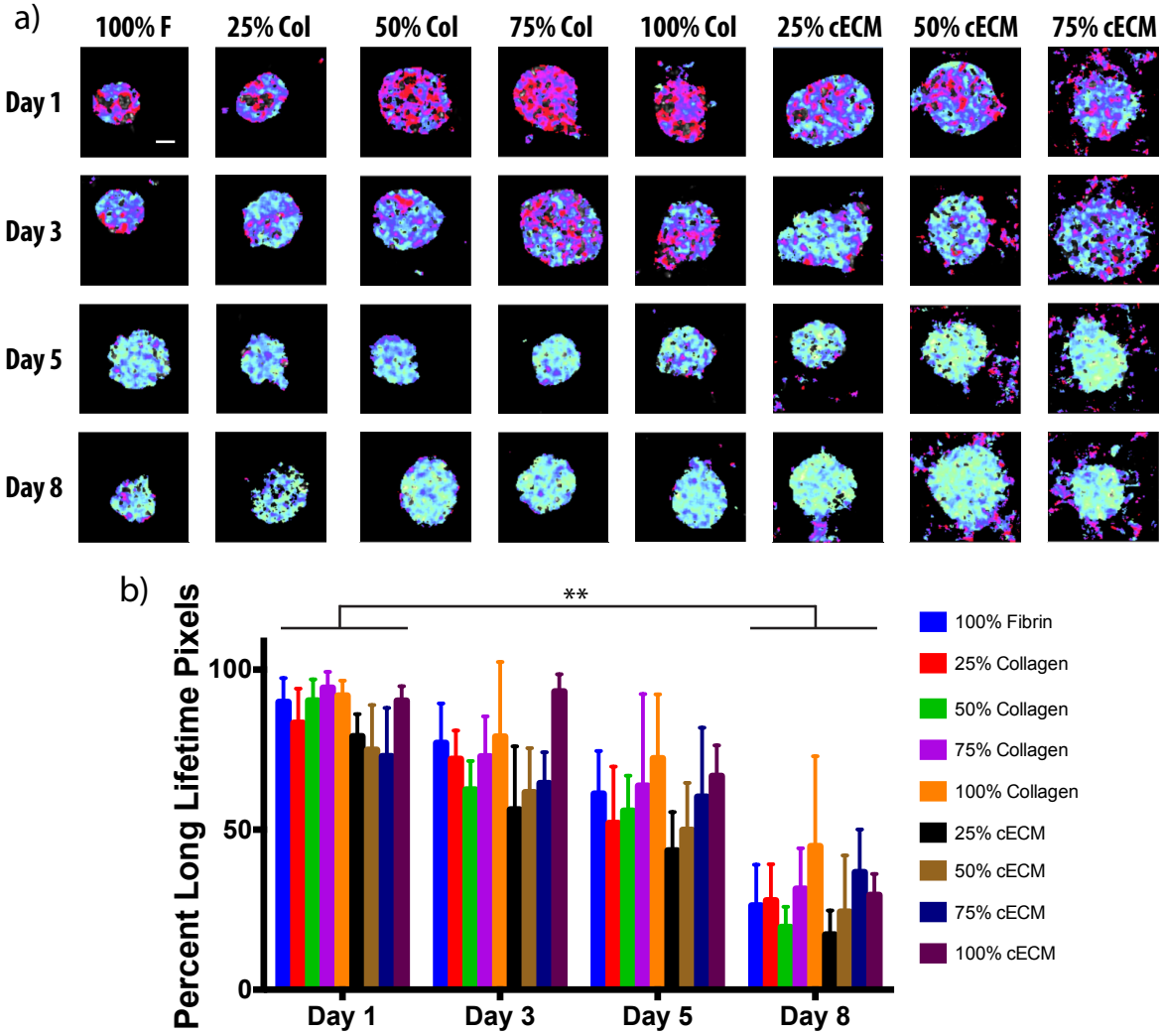


*Figure 3.3:* a) Phasor time-lapse FLIM captures the transient metabolic nature of cardiomyocyte spheroids embedded into extracellular matrix. Over time, iPS-CM spheroids shift towards a more glycolytic phenotype signified by a higher free/bound NADH ratio. Encapsulation within different types of matrices did not significantly effect the ratio of free:bound NADH. b) iPS-CM spheroids in all conditions shifted towards more free NADH as demonstrated by an average decrease of 7.78±1.53% long lifetime pixels/day. Long lifetime pixels significantly decreased from 84.94% ± 11.50% on Day 1 to 28.61% ± 15.91% on Day 8 (t-test, $P<0.0001$; F = Fibrin, Col = Collagen; scale bar = 25 μm)

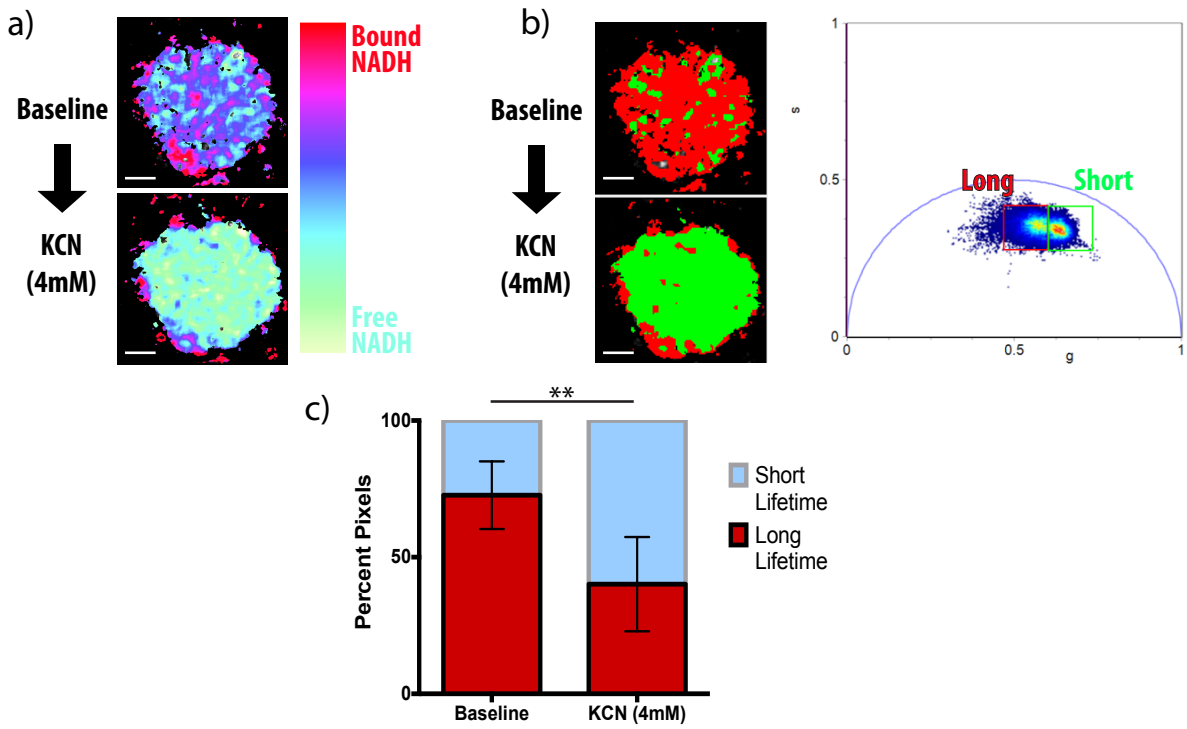


*Figure 3.4:* FLIM phasor characterization of metabolic poisoning by cyanide. a) FLIM phasor map of representative human iPS-CM spheroid before and after exposure to KCN (4mM). b) Corresponding FLIM map and phasor plot after thresholding pixels to long and short lifetime. C) KCN exposure significantly altered cardiac spheroid metabolism as long lifetime pixels decreased from 72.69% ± 12.36% to 40.13% ± 17.26% percent of total pixels (t-test, P<0.001). (scale bar = 25 μm)

## 3.5 Discussion

As *in vitro* testing platforms become more advanced, it is important to understand how different methodologies may affect cellular response. Switching from 2D cell culture to 3D culture has been previously shown to strongly alter *in vitro* function [96,97,275] and drug response [93-95,98,276]. As we improve the complexity of our cardiac drug screening platforms, it will be important to monitor the effects of different tissue engineering choices. In this work we transformed human iPS-CM grown in 2D monolayers into 3D cardiac spheroids and then embedded the spheroids into different compositions of extracellular matrices to monitor their phenotype. Our results demonstrate the effects of extracellular matrix

composition and time in culture on contractility, calcium handling and metabolism of cardiac spheroids.

Past research has shown that cardiomyocyte function improved when cultured in an environment similar to its native *in vivo* microenvironment [64,277]. Chemical decellularization of cardiac tissue creates a biomaterial with properties (e.g., composition) that more closely resembles the *in vivo* cardiac extracellular matrix that is composed primarily of collagen, laminin and elastin [67]. Collagen and fibrin gels were used as controls as collagen is the primary component of cECM with similar stiffness, while fibrin is notably absent from the heart. Collagen matrix reduced cardiac spheroid beating rate and slightly increased CTD90 in comparison to spheroids within pure fibrin gels, while cECM further reduced beating rate and greatly increased CTD90. Although contractility rates and calcium duration were altered by collagen and cECM, calcium amplitude of cardiac spheroids was not significantly affected by matrix composition. These results may suggest that stiffness and chemical cues of extracellular matrix may not play a role in l-type calcium channel expression or sarcoplasmic reticulum calcium storage.

Stem cell-derived cardiomyocyte phenotype has been widely reported to change over time. For drug screening purposes, it is crucial to understand the nature in which cardiomyocyte phenotype changes over time within each testing platform in order to properly interpret and compare cardiac drug response. Our results show iPS-CM function can change within a relatively short period of time (<2 Days) compared to the length of time at which iPS-CM can be cultured (>360 Days [278]). It may be necessary to allow cardiomyocyte phenotype to become stable when creating an iPS-CM-based platform to accurately model a response to external stimuli. Future work may be focused on creating

new tissue engineering methods to control and stabilize iPS-CM phenotype for *in vitro* cardiac drug screening.

Phasor FLIM is a promising tool to measure metabolic signatures for cardiac tissue applications. Current reports of stem cell-derived cardiomyocytes agree that cardiomyocytes resemble an immature phenotype, especially with respect to metabolism [48,279], while adult cardiomyocytes heavily depend on oxidative phosphorylation for ATP production [174,175]. iPS-CM cultured as monolayers were reported to increase ATP production and levels of mitochondrial oxidative phosphorylation over a period of 21 days [178]. In contrast, our phasor FLIM results indicated that human iPS-CM spheroids encapsulated in extracellular matrix increasingly rely on glycolysis for ATP production over a period of 8 days. Different matrix compositions had little effect on the metabolic shift towards more glycolysis, similar to calcium amplitude being unaffected. Recreating the cardiac niche with cECM did not induce metabolic maturation towards more oxidative phosphorylation and did not prevent the glycolytic shift within the time frame examined. Future experiments may be done to evaluate iPS-CM metabolism with FLIM phasor analysis over longer periods of time to compare culture in 2D to 3D.

In summary, we have characterized the effects of extracellular matrix encapsulation on human iPS-CM spheroid function with respect to contractility, calcium handling and metabolism over a period of 1 week. We conclude that collagen and cardiac ECM reduced beating rate and increased CTD90. Cardiac spheroid metabolism shifted towards a more glycolytic phenotype after encapsulation within extracellular matrix, which was not affected by matrix composition. FLIM phasor analysis can therefore be used to monitor transient changes in metabolic signature in cardiac tissue engineering applications. FLIM

analysis characterized the acute effect of cyanide poisoning, and therefore FLIM could be used as a tool to understand whether cardioactive drugs that affect contractility do so by modulating metabolism. The predictive capability of new cardiac drug screening platforms will depend on the ability to assay all effects of unknown drugs on important facets of cardiomyocyte function.

# CHAPTER 4

# Effects of interstitial flow on a model of vascularized cardiac tissue

## 4.1 Abstract

A method to rapidly mature stem cell-derived cardiomyocytes to an adult phenotype remains elusive. Recreation of the *in vivo* microenvironment may potentially transform the immature phenotype of stem-derived cardiomyocytes. Endothelial cells play a crucial role in the *in vivo* development of cardiomyocytes and may be the key to *in vitro* maturation of cardiomyocytes. Here we demonstrate a microfluidic device that supports the formation of a vascularized beating cardiac tissue. We examined the effect of interstitial flow on vascularization of cardiac tissue and the simultaneous effect on cardiomyocyte phenotype. Interstitial flow increased the vascularized network area and increased the rate of cardiac spheroid growth, but did not significantly effect cardiomyocyte calcium handling. Although interstitial flow improved the phenotype of the vascularized cardiac tissue, the mechanism may not be due to NO signaling. Our results suggest a synergistic effect of interstitial flow and vascular network formation on cardiomyocyte phenotype.

## 4.2 Introduction

*In vitro* maturation of stem cell-derived cardiomyocytes remains a necessary goal in order to realize their full potential for use in tissue engineering, disease modeling, biological studies and drug toxicity screening [280]. Cardiomyocytes derived from human stem cells phenotypically resemble fetal cardiomyocytes [2] which may less accurately replicate physiological response for drug screening purposes. Although simply culturing stem-cell derived cardiomyocytes for an extended period (>360 days) develops some facets of the adult phenotype [54], this method is impractical and more complex culture methods may be necessary to accelerate maturation. Novel methods to recapitulate the *in vivo* cardiac niche have induced maturation, including electrical stimulation [58,59], mechanical stimulation [46,62,65,66], and coculture [43].

Endothelial cells have been shown to be crucial for *in vivo* development of the heart. Both endothelial cells and cardiomyocytes differentiate from a common progenitor cell and develop concurrently within the embryo [281]. Reciprocal signaling between endothelial cells and cardiomyocytes influences myocardial growth, metabolism, contractility and rhythmicity [282]. In addition, deletion of endothelial-specific genes causes myocardial developmental defects including noncompaction, cardiomyopathy, thinned myocardium, chamber dilation and septal defects [283].

Endothelial cells are also important in the modulation of cardiomyocyte function. Damaging intact cardiac vascular endothelium reduces ventricular function by decreasing twitch duration, decreasing total tension and lowering the maximum velocity of muscle shortening [284]. In response to increased flow, coronary endothelial cells release endothelin which can increase the contractility of cardiac tissue [285]. Neuregulin production by

endothelial cells promotes cardiomyocyte proliferation, survival and growth [286]. Coculture of stem cell-derived cardiomyocytes with endothelial cells improves electrophysiology by upregulation of connexin43 [287].

A key component of the signaling pathway between endothelial cells and cardiomyocytes is the reactive oxygen species nitric oxide (NO) [288]. Endothelial cells are mechanically sensitive and increase NO production in response to increased shear stress [289-291]. Cardiomyocytes are inherently sensitive to NO and respond differently depending on the concentration of NO present [292]. Normal *in vivo* cardiac function relies on NO secreted by endothelial coronary cells, which increases diastolic volume and decreases duration of contraction necessary for high frequency pumping [293]. On a cellular level, NO induces relaxation of cardiomyocytes that is necessary for normal diastole function [61,294,295] and promotes cardiomyocytes to follow the frank-starling law [296]. Increased distensibility also activates endogenous autocrine eNOS, which increases sarcoplasmic reticulum calcium release, elevates intracellular calcium transient and strengthens contraction force [297]. Furthermore, endothelial angiogenesis promotes cardiomyocyte hypertrophy through an NO-mediated mechanism [298]. Endothelial NO promotes degradation of RGS4, a protein that inhibits the Gβγ/PI3Kγ/AKT/mTORC1 pathway known to control cardiomyocyte hypertrophy.

We hypothesized increased interstitial flow would increase endothelial NO production in an *in vitro* model of vasculogenesis. Consequently, increased NO availability would induce hypertrophy of human induced pluripotent stem (iPS) cell-derived cardiomyocytes cocultured within the developing vascular network. Here, we designed a microfluidic

device capable of controlling interstitial flow in an *in vitro* 3D co-culture model of vascularized human iPS cell-derived cardiomyocytes.

## 4.3 Methods

*Device fabrication*

The device is constructed of a polydimethylsiloxane (PDMS) slab plasma bonded to a glass slide similar to previous experiments [89]. Briefly, traditional photolithography techniques were used to create a patterned SU-8 design on a silicon wafer. The silicon wafer was silanized using trichlorosilane. A layer of PDMS was cast using the master mold on the silicon wafer to create a PDMS slab with desired features. The PDMS slab was removed from the wafer and holes were punched using a 23G needle. A glass slide then was then plasma bonded to the bottom of the PDMS slab to enclose the channels.

For electrical pacing experiments, the PDMS slab was bonded to a glass slide patterned with a thin film of interdigitated electrodes made of gold or indium tin oxide (ITO). The glass slides were coated with titanium (200 Å) and gold (1000 Å). The gold-covered slides were patterned using AZ 4620 photoresist. The titanium and gold layers were selectively removed with wet etching, and then subsequently the remaining photoresist was removed to reveal features of the interdigitated gold electrodes. An electrical pacing signal was generated using a Myopacer Cell Stimulator (Ion Optix). Biphasic square pulses of 1 ms duration at 1-5 V were used to control rhythmic contraction of the cardiac tissue.

The device design consists of a central tissue chamber (1 mm x 3 mm x 0.1 mm) with adjacent 100 μm wide microfluidic channels for delivery of growth medium. The central tissue chamber is connected to the microfluidic channels via three 30 μm wide pores

spaced 2 mm apart. Large reservoirs were attached to the ends of the microfluidic channels to create a hydrostatic pressure drop to control the rate and direction of convective interstitial flow. Flow within the device was calculated by finite element modeling in COMSOL Multiphysics 4.4. The pressure drop across the tissue and interstitial velocity ranged from 8.9 mm $H_2O$ and 3.4 µm/s (supraphysiological) for the condition of high flow (HF) and 4.2 mm $H_2O$ and 1.72 µm/s (physiological) for the condition of low flow (LF).

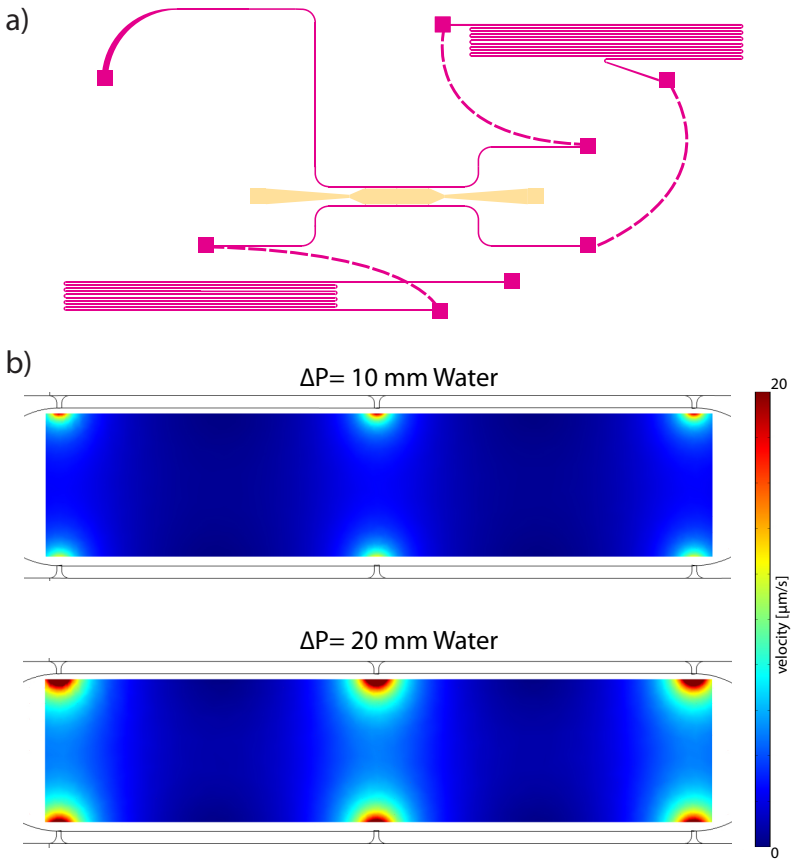


*Figure 4.1:* Microfluidic device design for vascularized cardiac tissue. (a) The microfluidic design consists of a central microtissue chamber (beige) with media delivered via adjacent microfluidic channels (solid pink lines) that are connected by three communication pores. Removable "jumper" connections (dotted pink lines) can be removed later to assist in tissue characterization with immunohistochemistry. (b) Finite element modeling of fluid velocity within the central chamber demonstrates change in velocity profile with respect to change in transverse pressure gradient across the microtissue chamber.

*Cardiac tissue formation and growth*

Wild-type human iPS cells (WTC-11 [270,271]) were provided as a gift from Dr. Bruce Conklin at the Gladstone Institute of Cardiovascular Disease, San Francisco. The WTC-11 iPS line was derived from a healthy male volunteer with a normal electrocardiodiagram and no known family history of cardiac disease [272]. For non-invasive calcium indication, the WTC-11 iPS line was genetically encoded with the ultrasensitive calcium protein sensor, GCaMP6f [273], through transcription activator-like effector nuclease (TALEN)-mediated genome editing [274]. The GcAMP6f protein consists of green fluorescent protein (GFP), the calcium-binding protein calmodulin (CaM), and the CaM-interacting M13 peptide. Calcium binding to the CaM-13 complex causes a conformational change in the protein complex, which increases the fluorescent intensity of the GFP. The fast green fluorescent indicator GCaMP6f under control of the constitutively expressed CAG promoter and puromycin antibiotic resistance gene under control of the endogenous promoter, were encoded into the AAVS1 locus of the WTC-11 iPS genome. Human iPS cells containing the GCaMP6f cassette were subsequently selected by puromycin (0.5 μg/mL). Differentiation of iPS cells into cardiomyocytes was performed using a small molecule-based Wnt modulating protocol [27]. Briefly, iPS cells were maintained with mTeSR1 (STEMCELL Technologies) in 6-well plates coated with Matrigel (BD Biosciences). At 80% confluence, iPS cells were dissociated with Accutase (Invitrogen) for 4 minutes at 37°C and plated (Day -4) onto 12-well plates coated with matrigel at a density of 33,000 cells/cm$^2$ in mTeSR1 with 10 μM Y-27632 (Tocris). The medium is replaced every 24 hours for 3 days (Day -3 to Day -1) with mTeSR1 only. On Day 0, differentiation of cells was initiated by canonical WNT activator 12 μM CHIR99021 (Selleck Chemicals) in RPMI 1640 medium supplemented with HEPES (Life

Technologies) and B27 supplement without insulin (Life Technologies). After 24 hours (Day 1), media is replaced with RPMI 1640 with B27 minus insulin only. On Day 3, cells are treated with Wnt inhibitor 5 μM IWP-2 (Tocris) in a 50:50 blend of conditioned media and fresh RPMI 1640 with B27 minus insulin. On Day 5, the media was replenished with RPMI 1640 with B27 minus insulin only. On Day 7 and every 2-3 days, the media is changed with RPMI 1640 with B27 with insulin. Beating cardiomyocytes (15-45 days old) were dissociated into single cells using 200 U/mL collagenase in Hank's balanced salt solution (Life Technologies) for 1 hour and then 0.25% trypsin/EDTA (Life Technologies) for 5 minutes at 37°C. Cells were then resuspended and seeded into AggreWell 400 (STEMCELL Technologies) plates at 300,000 cells per well. Human iPS-derived cardiomyocyte (iPS-CM) spheroids were allowed to aggregate, and then self-assembled for two days before seeding into the microfluidic device.

The cardiac tissue was formed similar to previous methods to create an *in vitro* vessel network within a device [89] with the addition of cardiac spheroids. Bovine fibrinogen (Sigma-Aldrich) was dissolved in Dulbecco's Phosphate Buffered Saline to a concentration of 10 mg fibrinogen/mL of solution. An Aggrewell of cardiac spheroids was split at a 1:8 ratio for each microfluidic device seeding. Normal human lung fibroblasts (NHLFs) and cord blood endothelial colony-forming cell-derived endothelial cells (ECFC-ECs) were mixed with the fibrinogen solution at a 2:1 ratio with a concentration of $7.5 \times 10^6$ cells/mL solution. The cellular-matrix mixture was used to resuspend the cardiac spheroids and then briefly mixed with thrombin for a final concentration of 3 U/mL before injection into the central tissue chamber to polymerize. The cardiac tissue chamber was maintained with fully supplemented endothelial growth medium-2 (EGM-2, Lonza) for 12 hours in a 20% $O_2$

incubator. The cardiac tissue chamber was switched to maintenance with EGM-2 media without basic fibroblast growth factor (bFGF) and vascular endothelial growth factor (VEGF) for two weeks in a 5% $O_2$ incubator. To modulate cellular NO production and NO availability, certain conditions were maintained with EGM-2 without bFGF and VEGF supplemented with combinations of L-NG-nitroarginine methyl ester (L-NAME) and S-Nitroso-L-glutathione (GSNO, Cayman Chemical).

*Nitric oxide quantification*

Device media was collected regularly to monitor cardiac tissue nitric oxide production. Media accumulated in the outlet reservoir for two days before collection. A fluorometric nitric oxide assay kit (Abcam) was used to prepare collected media for quantification. A fluorescent plate reader (SpectraMax) was used to measure the fluorescent intensity of nitric oxide probe. Nitric oxide generation rate was calculated with the following steady-state equation:

$$\dot{V}_{tiss} C_{NO,in} - \dot{V}_{tiss} C_{NO,out} + r_{NO} V_{tissue} = 0$$

where $\dot{V}_{tiss}$ is the volumetric flow through the tissue, $C_{NO}$ is the NO concentration entering the tissue or leaving the tissue, $r_{NO}$ is the volumetric generation rate of NO within the tissue and $V_{tiss}$ is the volume of the tissue. The equation can be rearranged to:

$$r_{NO} = \frac{\dot{V}_{tiss} C_{NO,out}}{V_{tiss}} .$$

As simulated by COMSOL, the volumetric flows under LF and HF conditions were 35 and 70 μL/day, respectively. The volume of the tissue was measured to be 0.6 $mm^3$. Mass flow balance of the outlet reservoir can be described as:

$$\dot{V}_{tiss} C_{NO,out} = \dot{V}_{res} C_{NO,res}$$

where $\dot{V}_{res}$ is the volumetric flow of liquid accumulating in the reservoir, and $C_{NO,res}$ is the concentration of NO in the reservoir that is collected an analyzed. The volumetric generation of NO within the cardiac tissue can therefore be reduced to:

$$r_{NO} = \frac{\dot{V}_{res} C_{NO,res}}{V_{tiss}} .$$

Volumetric flows of for LF and HF conditions as simulated by COMSOL were 114.91 and 252.29 μL/day, respectively.

*Cardiomyocyte calcium transient analyses*

Calcium transients of cardiomyocyte spheroids were analyzed by visually recording fluorescent activity of GCaMP6 during spheroid contractions. Videos were taken at 15.65 Hz using MetaMorph software (Molecular Devices) with an Olympus IX83 inverted microscope (Olympus) connected to a black and white CCD digital camera (Hamamatsu). Videos were saved as a TIFF stack and imported into ImageJ (NIH). A ROI was applied over each frame of the video to measure the average pixel intensity of only the spheroid. Excel was used to quantify calcium amplitude, which is defined as the difference between intensity of the spheroid in a relaxed state and the maximum intensity when contracted.

*Immunofluorescent staining and image analyses*

Vascularized cardiac tissues were immunofluorescently stained using rabbit anti-human cTnT antibody (Abcam), mouse anti-human CD31 antibody (Dako), goat anti-rabbit IgG Alexa Fluor 488 secondary antibody (Life Technologies) and goat anti-mouse IgG Alexa Fluor 555 secondary antibody (Life Technologies). The tissues were prepared for immunostaining by fixing the tissues with formalin for 8 hours. Blocking, washing and antibody incubation were performed by flowing corresponding solutions through the microfluidic channels for 1-2 days. The devices were imaged using an Olympus IX83 inverted microscope. Vessel networks were characterized and quantified using the software Angiotool [299].

*Statistical significance*

Student's t-test was performed where a p-value $< 0.05$ was considered significant. The data are expressed as mean ± standard deviation.

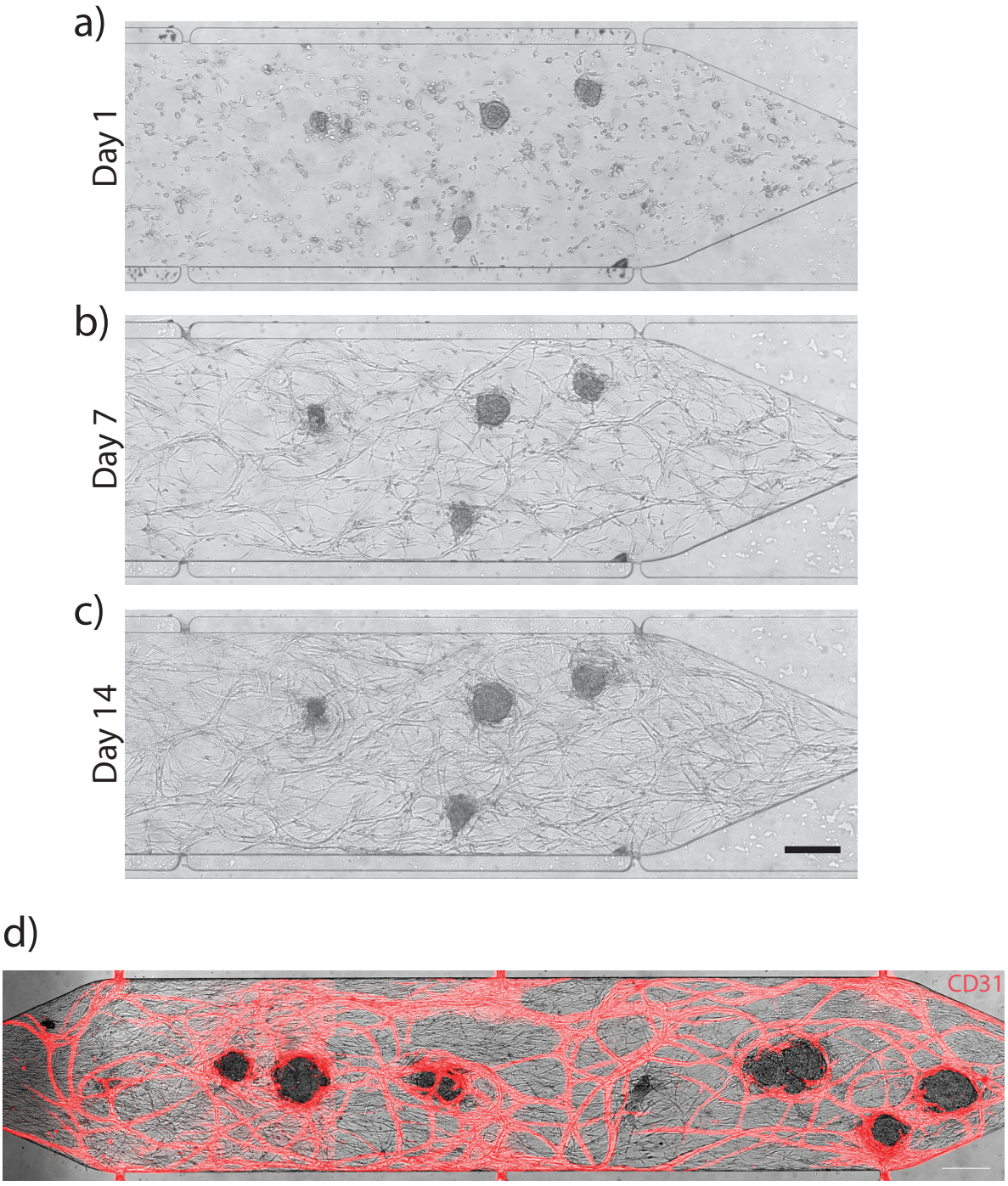


*Figure 4.2:* Growth of a vascular network surrounding human iPS-derived cardiomyocyte spheroids within the central microfluidic chamber. a) Human iPS-CM spheroids were seeded with ECFCs and NHFLs on day 1. Dark spots indicate dense human iPS cardiac spheroids. b) By week 1, cardiac spheroids grew in place while surrounding cells underwent vasculogenesis. c) By week 2, a fully interconnected vascular network formed in the presence of the human cardiomyocyte spheroids. (scale bar = 250 μm) d) Immunofluorescent image of CD31 positive cells demonstrate a developed vessel network which spans the entire device after 14 days overlayed with a bright field image.

## 4.4 Results

We designed and constructed a PDMS microfluidic device with outer microfluidic channels delivering media to a central tissue chamber via three communication pores each side (Fig. 4.1a). To analyze the effects of interstitial flow on vascular development of the cardiac tissue, a hydrostatic pressure gradient across the tissue chamber was varied between a low flow condition (LF) of 10 mm of $H_2O$ and a high flow condition (HF) of 20mm of $H_2O$ to generate an average interstitial velocity of 1.72 and 3.43 μm/s, respectively (Fig. 4.1b). Over 14 days, the ECFC-ECs, cocultured with NHLFs, developed into an interconnected vessel network that surrounded the adjacent human iPS-CM spheroids (Fig. 4.2).

To understand the relationship of interstitial flow and nitric oxide on vessel network formation, vascularized cardiac tissues were subject to low and high interstitial flows, and exposed to a NOS inhibitor (L-NAME) or a nitric oxide donor (GSNO). Measured nitric oxide levels had significant variations within each experimental condition. Increased interstitial flow reduced vascularized cardiac tissue NO production rate from 1716.2 ± 1083.0 pmol NO/$mm^3$ tissue/day to 866.1 ± 607.9 pmol NO/$mm^3$ tissue/day (Fig. 3a). Under HF conditions, addition of a nitric oxide donor in the presence of the NOS inhibitor increased NO concentration from 1061.8 ± 711.4 to 1607.3 ± 958.4 pmol NO/$mm^3$ tissue/day. Increased hydrostatic pressure and interstitial velocity resulted in greater vessel network area coverage of the tissue chamber from 24.65% ± 10.11% (LF) to 31.63% ± 7.73% (HF) (Fig. 4.3b). Modulation of NO did not significantly effect vessel network formation.

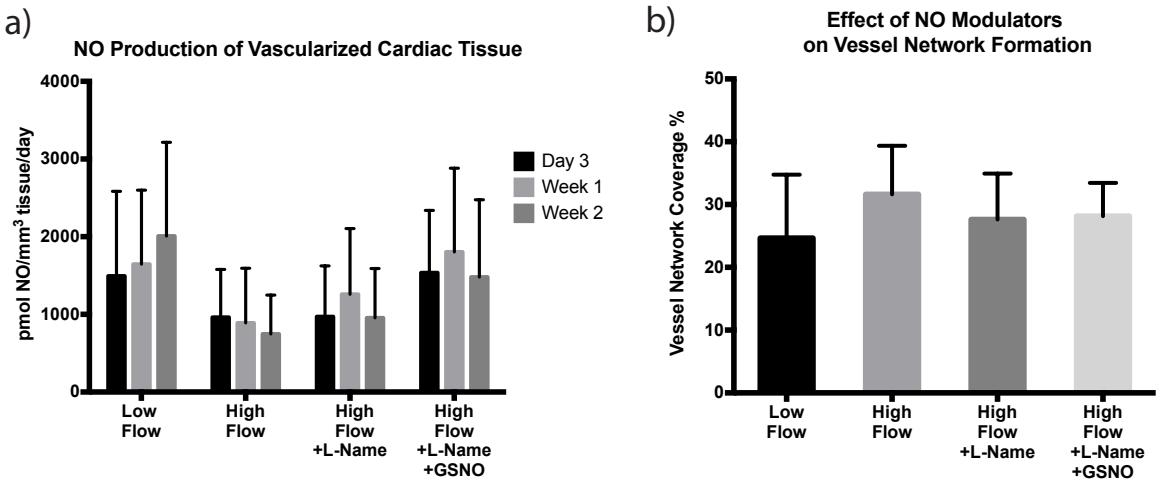


*Figure 4.3*: Effect of interstitial flow on NO production and endothelial network formation. a) Vascularized cardiac tissue produced different amounts of NO in response to change in hydrostatic pressure and exposure to NO modulators. b) Corresponding changes in vessel network formation within the cardiac tissue was also affected by similar manipulations in mechanical and chemical cues.

Cardiomyocytes regained spontaneous contraction within 1-3 days of loading into the device. All cardiac spheroids grew in size over time in culture (Fig. 4.4a). Increased interstitial flow significantly increased the amount of growth from 87.48% ± 41.52% (LF) to 179.25% ± 128.1% ($P < 0.028$; Fig. 4.4b). Modulation of NO did not significantly affect growth of spheroids under HF conditions. Cardiac spheroid calcium handling was measured by recording GCaMP6 fluorescence during contraction (Fig. 4.4c,d). Increased interstitial increased cardiac spheroid calcium amplitude immediately after seeding into the device, but did not have significant effects thereafter (Fig. 4.4e).

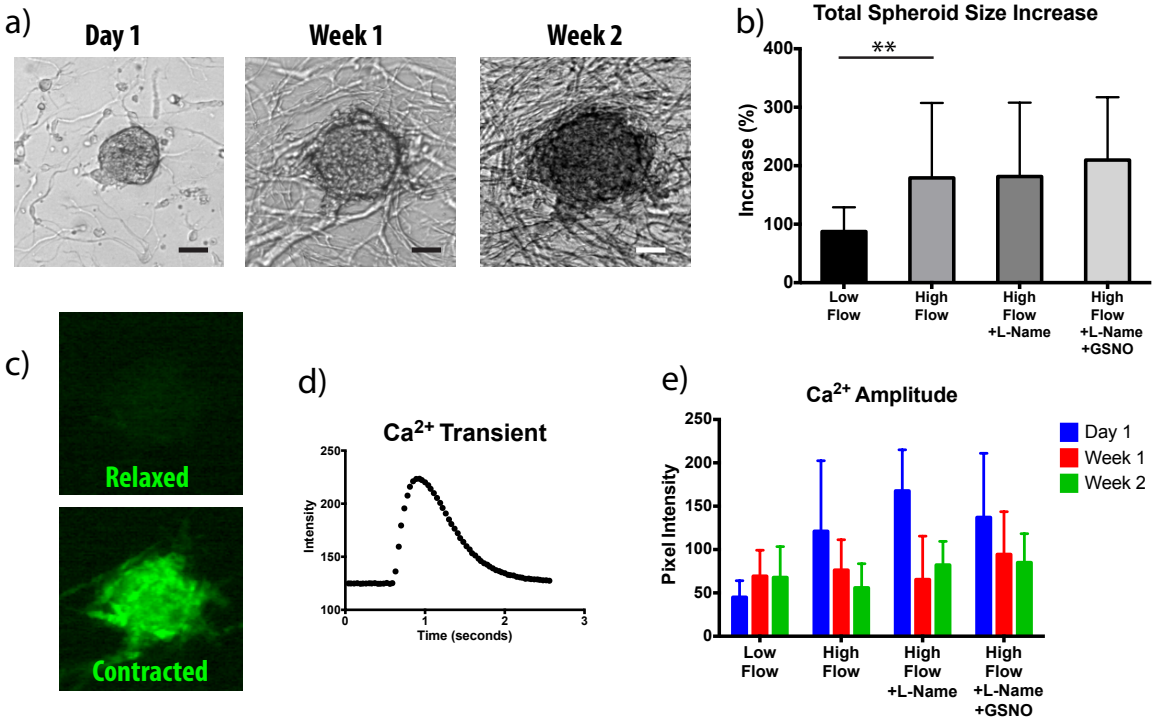


*Figure 4.4:* Effect of interstitial flow on cardiomyocyte phenotype. a) Human iPS-CM spheroids grew over a period of 2 weeks when cocultured with ECFC-ECs and NHFLs within the microfluidic device (scale bar = 50 μm). b) High interstitial flow significantly increased cardiac spheroid growth from 87.48% ± 41.52% (LF) to 179.25% ± 128.1% ($P < 0.028$). NO modulators did not have a significant effect on spheroid growth. c) Green fluorescence of the calcium indicator protein GCaMP6 increased intensity when the cardiac spheroids contracted. d) Intensity of green fluorescence over time corresponded to the ability of cardiac spheroids to rapidly cycle intracellular calcium levels. e) High interstitial flow increased magnitude of calcium amplitude on day one, but did not have a significant effect on cardiomyocyte calcium amplitude on subsequent time points.

## 4.5 Discussion

In this work, we demonstrated the capability of our microfluidic device for the creation and culture of beating cardiac tissues that develop a vascular network via vasculogenesis. Our device was designed for precise control of nutrient delivery and can be used to simultaneously study the effects of coculture and fluid flow. Increased interstitial velocity decreased NO production, counter to our hypothesis, but still resulted in larger vascular network formation and increased cardiac spheroid growth, potentially indicative of cardiac hypertrophy. NO modulators did not significantly affect vascular network formation,

cardiomyocyte growth or cardiomyocyte calcium handling. Therefore, the effects at which interstitial flow influences improved vascularization and cardiac growth may be due to another mechanism rather than NO signaling.

Although the results from this study incorporate flow rates considered to be physiological and superphysiological, a larger difference between flow rates (>1 order of magnitude) may be needed to induce more significant changes. Physiological interstitial flow velocities range between 0.1 to 2 μm/s [300]. Future microfluidic designs can incorporate the extremities of interstitial velocities to better examine the effect on vascular cardiac tissue phenotype. To compare a large range interstitial flows, careful consideration will be required to do design a device with constant nutrient delivery independent of flow rate.

The device was designed to establish nutrient gradients throughout the tissue and create areas of metabolic deficits to encourage self-assembly of ECFC-ECs into a vascular network. For our experiments, we chose to use cardiac spheroids to insert dense tissue that would continue the theme of metabolic demand. Due to the nature of seeding the cells into the device, cardiac spheroids were seeded in a wide range from 1 spheroid up to 15 spheroids per tissue. The wide distribution of our results may be due to the variability of cardiac cells present. Rather than create tissues from spheroids, future experiments may instead create areas of metabolic need by loading large amounts of single cell cardiomyocytes for improved consistency and potentially more significant results.

In summary, we have shown the potential of altering interstitial flow rate to improve vessel network formation of cardiac tissue. We conclude that nitric oxide may not be the mechanism at which interstitial flow improves network formation and cardiomyocyte

spheroid growth. New understandings of the interplay between the endothelial network and cardiomyocytes may lead to new methodologies to mature stem cell-derived cardiomyocytes, which would open their potential for use in biological testing, cardiac drug screening and cellular therapies.

# References


1 Dong, C. Y. *et al.* Fluorescence-lifetime imaging techniques for microscopy. *Methods Cell Biol* **72**, 431-464 (2003).

2 Robertson, C., Tran, D. D. & George, S. C. Concise Review: Maturation Phases of Human Pluripotent Stem Cell-Derived Cardiomyocytes. *Stem Cells* **31**, 829-837 (2013).

3 Wright, B. K. *et al.* NADH distribution in live progenitor stem cells by phasor-fluorescence lifetime image microscopy. *Biophys J* **103**, L7-L9 (2012).

4 Murphy, S. L., Xu, J. & Kochanek, K. D. Deaths: final data for 2010. *National Vital Statistics Reports* **61**, 1-118 (2013).

5 Control, C. f. D. & Prevention. (2011).

6 Go, A. S. *et al.* Heart disease and stroke statistics--2014 update: a report from the American Heart Association. *Circulation* **129**, e28 (2014).

7 Unit, E. S. Efficacy and safety of cholesterol-lowering treatment: prospective meta-analysis of data from 90 056 participants in 14 randomised trials of statins. *Lancet* **366**, 1267-1278 (2005).

8 Libby, P., Ridker, P. M. & Maseri, A. Inflammation and atherosclerosis. *Circulation* **105**, 1135-1143 (2002).

9 Roivainen, M. *et al.* Infections, inflammation, and the risk of coronary heart disease. *Circulation* **101**, 252-257 (2000).

10 Blanco-Colio, L. M., Tu√±√≥n, J., Mart√≠n-Ventura, J. L. & Egido, J. s. Anti-inflammatory and immunomodulatory effects of statins. *Kidney international* **63**, 12-23 (2003).

11 Chobanian, A. V. *et al.* The seventh report of the joint national committee on prevention, detection, evaluation, and treatment of high blood pressure: the JNC 7 report. *Jama* **289**, 2560-2571 (2003).

12 Friedman, M. A. *et al.* The safety of newly approved medicines: do recent market removals mean there is a problem? *Jama* **281**, 1728-1734 (1999).

13 DiMasi, J. A., Hansen, R. W. & Grabowski, H. G. The price of innovation: new estimates of drug development costs. *Journal of health economics* **22**, 151-185 (2003).

14 Adams, C. P. & Brantner, V. V. Estimating the cost of new drug development: is it really $802 million? *Health Affairs* **25**, 420-428 (2006).

15 Sondergaard, J., Wadskov, S., Jensen, H. A. & Mikkelsen, H. Aggravation of psoriasis and occurrence of psoriasiform cutaneous eruptions induced by practolol (Eraldin). *Acta dermato-venereologica* **56**, 239-243 (1975).

16 Oliver, M. *et al.* WHO cooperative trial on primary prevention of ischaemic heart disease with clofibrate to lower serum cholesterol: final mortality follow-up. *Lancet*, 600-604 (1984).

17 Berg, F. M. Health risks associated with weight loss and obesity treatment programs. *Journal of Social Issues* **55**, 277-297 (1999).

18 Wysowski, D. K. & Bacsanyi, J. Cisapride and fatal arrhythmia. *New England Journal of Medicine* **335**, 290-291 (1996).

19 Graham, D. J. *et al.* Risk of acute myocardial infarction and sudden cardiac death in patients treated with cyclo-oxygenase 2 selective and non-selective non-steroidal anti-inflammatory drugs: nested case-control study. *The Lancet* **365**, 475-481 (2005).

20 Kelly, H. G., Fay, J. & Laverty, S. Thioridazine hydrochloride (Mellaril): its effect on the electrocardiogram and a report of two fatalities with electrocardiographic abnormalities. *Canadian Medical Association Journal* **89**, 546 (1963).

21 Sturner, W. Q. & Garriott, J. C. Deaths involving propoxyphene: A study of 41 cases over a two-year period. *Jama* **223**, 1125-1130 (1973).

22 Nissen, S. E. & Wolski, K. Effect of rosiglitazone on the risk of myocardial infarction and death from cardiovascular causes. *New England Journal of Medicine* **356**, 2457-2471 (2007).

23 Takahashi, K. *et al.* Induction of pluripotent stem cells from adult human fibroblasts by defined factors. *cell* **131**, 861-872 (2007).

24 Zhang, J. *et al.* Functional Cardiomyocytes Derived From Human Induced Pluripotent Stem Cells. *Circulation Research* **104**, e30-e41, doi:10.1161/circresaha.108.192237 (2009).

25 Dimos, J. T. *et al.* Induced pluripotent stem cells generated from patients with ALS can be differentiated into motor neurons. *Science* **321**, 1218-1221 (2008).

26 Zhang, J. *et al.* Extracellular Matrix Promotes Highly Efficient Cardiac Differentiation of Human Pluripotent Stem CellsNovelty and Significance The Matrix Sandwich Method. *Circulation research* **111**, 1125-1136 (2012).
27 Lian, X. *et al.* Robust cardiomyocyte differentiation from human pluripotent stem cells via temporal modulation of canonical Wnt signaling. *Proceedings of the National Academy of Sciences* **109**, E1848-E1857 (2012).
28 Rana, P., Anson, B., Engle, S. & Will, Y. Characterization of human induced pluripotent stem cell derived cardiomyocytes: bioenergetics and utilization in safety screening. *Toxicological Sciences*, kfs233 (2012).
29 Sirenko, O. *et al.* Assessment of beating parameters in human induced pluripotent stem cells enables quantitative in vitro screening for cardiotoxicity. *Toxicology and applied pharmacology* **273**, 500-507 (2013).
30 Tanaka, T. *et al.* < i> In vitro</i> pharmacologic testing using human induced pluripotent stem cell-derived cardiomyocytes. *Biochemical and biophysical research communications* **385**, 497-502 (2009).
31 Yokoo, N. *et al.* The effects of cardioactive drugs on cardiomyocytes derived from human induced pluripotent stem cells. *Biochem Biophys Res Commun* **387**, 482-488, doi:S0006-291X(09)01394-1 [pii]
10.1016/j.bbrc.2009.07.052 (2009).
32 Moretti, A. *et al.* Patient-specific induced pluripotent stem-cell models for long-QT syndrome. *New England Journal of Medicine* **363**, 1397-1409 (2010).
33 Itzhaki, I. *et al.* Modelling the long QT syndrome with induced pluripotent stem cells. *Nature* **471**, 225-229 (2011).
34 Malan, D., Friedrichs, S., Fleischmann, B. K. & Sasse, P. Cardiomyocytes obtained from induced pluripotent stem cells with long-QT syndrome 3 recapitulate typical disease-specific features in vitro. *Circulation research* **109**, 841-847 (2011).
35 Lahti, A. L. *et al.* Model for long QT syndrome type 2 using human iPS cells demonstrates arrhythmogenic characteristics in cell culture. *Disease models & mechanisms* **5**, 220-230 (2012).
36 Ma, Z. *et al.* Three-dimensional filamentous human diseased cardiac tissue model. *Biomaterials* **35**, 1367-1377 (2014).
37 Fatima, A. *et al.* In vitro modeling of ryanodine receptor 2 dysfunction using human induced pluripotent stem cells. *Cellular Physiology and Biochemistry* **28**, 579-592 (2011).
38 Carvajal-Vergara, X. *et al.* Patient-specific induced pluripotent stem-cell-derived models of LEOPARD syndrome. *Nature* **465**, 808-812 (2010).
39 Ohler, A. *et al.* Two-photon laser scanning microscopy of the transverse-axial tubule system in ventricular cardiomyocytes from failing and non-failing human hearts. *Cardiology research and practice* **2009** (2010).
40 Lieu, D. K. *et al.* Absence of transverse tubules contributes to non-uniform Ca2+ wavefronts in mouse and human embryonic stem cell-derived cardiomyocytes. *Stem cells and development* **18**, 1493-1500 (2009).
41 Snir, M. *et al.* Assessment of the ultrastructural and proliferative properties of human embryonic stem cell-derived cardiomyocytes. *American Journal of Physiology-Heart and Circulatory Physiology* **285**, H2355-H2363 (2003).
42 Xu, X. Q., Soo, S. Y., Sun, W. & Zweigerdt, R. Global expression profile of highly enriched cardiomyocytes derived from human embryonic stem cells. *Stem Cells* **27**, 2163-2174, doi:10.1002/stem.166 (2009).
43 Kim, C. *et al.* Non-cardiomyocytes influence the electrophysiological maturation of human embryonic stem cell-derived cardiomyocytes during differentiation. *Stem cells and development* **19**, 783-795 (2009).
44 Wang, K. *et al.* Biophysical properties of slow potassium channels in human embryonic stem cell derived cardiomyocytes implicate subunit stoichiometry. *The Journal of physiology* **589**, 6093-6104 (2011).
45 Hoekstra, M., Mummery, C. L., Wilde, A. A., Bezzina, C. R. & Verkerk, A. O. Induced pluripotent stem cell derived cardiomyocytes as models for cardiac arrhythmias. *Frontiers in physiology* **3** (2012).
46 Foldes, G. *et al.* Modulation of human embryonic stem cell-derived cardiomyocyte growth: A testbed for studying human cardiac hypertrophy? *Journal of Molecular and Cellular Cardiology* **50**, 367-375, doi:Doi 10.1016/J.Yjmcc.2010.10.029 (2011).
47 Satin, J. *et al.* Mechanism of spontaneous excitability in human embryonic stem cell derived cardiomyocytes. *The Journal of physiology* **559**, 479-496 (2004).
48 Hattori, F. *et al.* Nongenetic method for purifying stem cell-derived cardiomyocytes. *Nat Methods* **7**, 61-66, doi:nmeth.1403 [pii]
10.1038/nmeth.1403.

49 Abu-Issa, R. & Kirby, M. L. Heart field: from mesoderm to heart tube. *Annu. Rev. Cell Dev. Biol.* **23**, 45-68 (2007).
50 Bird, S. *et al.* The human adult cardiomyocyte phenotype. *Cardiovascular research* **58**, 423-434 (2003).
51 Snir, M. *et al.* Assessment of the ultrastructural and proliferative properties of human embryonic stem cell-derived cardiomyocytes. *Am J Physiol Heart Circ Physiol* **285**, H2355-2363, doi:10.1152/ajpheart.00020.2003
285/6/H2355 [pii] (2003).
52 Lundy, S. D., Zhu, W.-Z., Regnier, M. & Laflamme, M. A. Structural and functional maturation of cardiomyocytes derived from human pluripotent stem cells. *Stem cells and development* **22**, 1991-2002 (2013).
53 Sartiani, L. *et al.* Developmental changes in cardiomyocytes differentiated from human embryonic stem cells: a molecular and electrophysiological approach. *Stem Cells* **25**, 1136-1144, doi:2006-0466 [pii]
10.1634/stemcells.2006-0466 (2007).
54 Kamakura, T. *et al.* Ultrastructural Maturation of Human-Induced Pluripotent Stem Cell-Derived Cardiomyocytes in a Long-Term Culture. *Circulation journal: official journal of the Japanese Circulation Society* (2013).
55 Moore, K. L., Torchia, M. G. & Persaud, T. *The Developing Human: Clinically Oriented Embryology With STUDENT CONSULT Online Access, 9/e*. (Elsevier India, 2007).
56 Joyner, R. W. & Van Capelle, F. Propagation through electrically coupled cells. How a small SA node drives a large atrium. *Biophys J* **50**, 1157-1164 (1986).
57 Severs, N. J. The cardiac muscle cell. *Bioessays* **22**, 188-199 (2000).
58 Nunes, S. S. *et al.* Biowire: a platform for maturation of human pluripotent stem cell-derived cardiomyocytes. *Nature methods* **10**, 781-+, doi:Doi 10.1038/Nmeth.2524 (2013).
59 Miklas, J. W. *et al.* Bioreactor for modulation of cardiac microtissue phenotype by combined static stretch and electrical stimulation. *Biofabrication* **6**, 024113 (2014).
60 Banerjee, I., Fuseler, J. W., Price, R. L., Borg, T. K. & Baudino, T. A. Determination of cell types and numbers during cardiac development in the neonatal and adult rat and mouse. *American Journal of Physiology-Heart and Circulatory Physiology* **293**, H1883-H1891 (2007).
61 Balligand, J.-L., Feron, O. & Dessy, C. eNOS activation by physical forces: from short-term regulation of contraction to chronic remodeling of cardiovascular tissues. *Physiological Reviews* **89**, 481-534 (2009).
62 Tulloch, N. L. *et al.* Growth of engineered human myocardium with mechanical loading and vascular coculture. *Circ Res* **109**, 47-59, doi:CIRCRESAHA.110.237206 [pii]
10.1161/CIRCRESAHA.110.237206.
63 Ingber, D. E. Tensegrity-based mechanosensing from macro to micro. *Progress in biophysics and molecular biology* **97**, 163-179 (2008).
64 Engler, A. J. *et al.* Embryonic cardiomyocytes beat best on a matrix with heart-like elasticity: scar-like rigidity inhibits beating. *Journal of cell science* **121**, 3794-3802 (2008).
65 Shimko, V. F. & Claycomb, W. C. Effect of mechanical loading on three-dimensional cultures of embryonic stem cell-derived cardiomyocytes. *Tissue Engineering Part A* **14**, 49-58 (2008).
66 Mihic, A. *et al.* The effect of cyclic stretch on maturation and 3D tissue formation of human embryonic stem cell-derived cardiomyocytes. *Biomaterials* **35**, 2798-2808 (2014).
67 Singelyn, J. M. *et al.* Catheter-deliverable hydrogel derived from decellularized ventricular extracellular matrix increases endogenous cardiomyocytes and preserves cardiac function post-myocardial infarction. *Journal of the American College of Cardiology* **59**, 751-763 (2012).
68 Sa, S., Wong, L. & McCloskey, K. E. Combinatorial Fibronectin and Laminin Signaling Promote Highly Efficient Cardiac Differentiation of Human Embryonic Stem Cells. *BioResearch Open Access* **3**, 150-161 (2014).
69 Duan, Y. *et al.* Hybrid Gel Composed of Native Heart Matrix and Collagen Induces Cardiac Differentiation of Human Embryonic Stem Cells without Supplemental Growth Factors. *J Cardiovasc Transl Res*, doi:10.1007/s12265-011-9304-0.
70 Unger, M. A., Chou, H.-P., Thorsen, T., Scherer, A. & Quake, S. R. Monolithic microfabricated valves and pumps by multilayer soft lithography. *Science* **288**, 113-116 (2000).
71 Whitesides, G. M. The origins and the future of microfluidics. *Nature* **442**, 368-373 (2006).
72 Keenan, T. M. & Folch, A. Biomolecular gradients in cell culture systems. *Lab Chip* **8**, 34-57 (2008).
73 Jeon, N. L. *et al.* Generation of solution and surface gradients using microfluidic systems. *Langmuir* **16**, 8311-8316 (2000).

74 Chung, B. G. *et al.* Human neural stem cell growth and differentiation in a gradient-generating microfluidic device. *Lab Chip* **5**, 401-406 (2005).
75 Hsu, Y.-H., Moya, M. L., Hughes, C. C., George, S. C. & Lee, A. P. A microfluidic platform for generating large-scale nearly identical human microphysiological vascularized tissue arrays. *Lab Chip* **13**, 2990-2998 (2013).
76 Stone, H. A., Stroock, A. D. & Ajdari, A. Engineering flows in small devices: microfluidics toward a lab-on-a-chip. *Annu. Rev. Fluid Mech.* **36**, 381-411 (2004).
77 Zhang, W. *et al.* PMMA/PDMS valves and pumps for disposable microfluidics. *Lab Chip* **9**, 3088-3094 (2009).
78 Pan, T., McDonald, S. J., Kai, E. M. & Ziaie, B. A magnetically driven PDMS micropump with ball check-valves. *Journal of Micromechanics and Microengineering* **15**, 1021 (2005).
79 Jeon, N. L. *et al.* Microfluidics section: design and fabrication of integrated passive valves and pumps for flexible polymer 3-dimensional microfluidic systems. *Biomedical Microdevices* **4**, 117-121 (2002).
80 Cha, J. *et al.* A highly efficient 3D micromixer using soft PDMS bonding. *Journal of Micromechanics and Microengineering* **16**, 1778 (2006).
81 Stroock, A. D. *et al.* Chaotic mixer for microchannels. *Science* **295**, 647-651 (2002).
82 Nguyen, N.-T. & Wu, Z. Micromixers,Äîa review. *Journal of Micromechanics and Microengineering* **15**, R1 (2005).
83 Johnson, T. J., Ross, D. & Locascio, L. E. Rapid microfluidic mixing. *Analytical Chemistry* **74**, 45-51 (2002).
84 Haswell, S. J. *et al.* The application of micro reactors to synthetic chemistry. *Chemical Communications*, 391-398 (2001).
85 McCreedy, T. & Wilson, N. G. Microfabricated reactors for on-chip heterogeneous catalysis. *Analyst* **126**, 21-23 (2001).
86 Berger, M., Castelino, J., Huang, R., Shah, M. & Austin, R. H. Design of a microfabricated magnetic cell separator. *ELECTROPHORESIS* **22**, 3883 (2001).
87 Neuzil, P., Giselbrecht, S., Lange, K., Huang, T. J. & Manz, A. Revisiting lab-on-a-chip technology for drug discovery. *Nature Reviews Drug Discovery* **11**, 620-632 (2012).
88 Dittrich, P. S. & Manz, A. Lab-on-a-chip: microfluidics in drug discovery. *Nature Reviews Drug Discovery* **5**, 210-218 (2006).
89 Moya, M. L., Hsu, Y.-H., Lee, A. P., Hughes, C. C. W. & George, S. C. In vitro perfused human capillary networks. *Tissue Engineering Part C: Methods* **19**, 730-737 (2013).
90 Kim, S., Lee, H., Chung, M. & Jeon, N. L. Engineering of functional, perfusable 3D microvascular networks on a chip. *Lab on a Chip* **13**, 1489-1500 (2013).
91 Sung, J. H. & Shuler, M. L. A micro cell culture analog (¬µCCA) with 3-D hydrogel culture of multiple cell lines to assess metabolism-dependent cytotoxicity of anti-cancer drugs. *Lab Chip* **9**, 1385-1394 (2009).
92 Sung, J. H., Kam, C. & Shuler, M. L. A microfluidic device for a pharmacokinetic,Äìpharmacodynamic (PK,ÄìPD) model on a chip. *Lab Chip* **10**, 446-455 (2010).
93 Weigelt, B., Lo, A. T., Park, C. C., Gray, J. W. & Bissell, M. J. HER2 signaling pathway activation and response of breast cancer cells to HER2-targeting agents is dependent strongly on the 3D microenvironment. *Breast cancer research and treatment* **122**, 35-43 (2010).
94 Tung, Y.-C. *et al.* High-throughput 3D spheroid culture and drug testing using a 384 hanging drop array. *Analyst* **136**, 473-478 (2011).
95 Horning, J. L. *et al.* 3-D tumor model for in vitro evaluation of anticancer drugs. *Molecular pharmaceutics* **5**, 849-862 (2008).
96 Kim, J. B., Stein, R. & O'Hare, M. J. Three-dimensional in vitro tissue culture models of breast cancer—a review. *Breast cancer research and treatment* **85**, 281-291 (2004).
97 Thomas, R. J. *et al.* The effect of three-dimensional co-culture of hepatocytes and hepatic stellate cells on key hepatocyte functions in vitro. *Cells Tissues Organs*, 67-79 (2005).
98 Pickl, M. & Ries, C. H. Comparison of 3D and 2D tumor models reveals enhanced HER2 activation in 3D associated with an increased response to trastuzumab. *Oncogene* **28**, 461-468 (2009).
99 Moya, M. L., Hsu, Y. H., Lee, A. P., Hughes, C. C. W. & George, S. C. In Vitro Perfused Human Capillary Networks. *Tissue Eng Part C-Me* **19**, 730-737, doi:Doi 10.1089/Ten.Tec.2012.0430 (2013).
100 Maidhof, R. *et al.* Biomimetic perfusion and electrical stimulation applied in concert improved the assembly of engineered cardiac tissue. *J Tissue Eng Regen M* **6**, e12-e23, doi:Doi 10.1002/Term.525 (2012).

101 Xiao, Y. *et al.* Microfabricated perfusable cardiac biowire: a platform that mimics native cardiac bundle. *Lab Chip* **14**, 869-882, doi:Doi 10.1039/C3lc51123e (2014).
102 So, J.-H. & Dickey, M. D. Inherently aligned microfluidic electrodes composed of liquid metal. *Lab on a Chip* **11**, 905-911 (2011).
103 WEN, X.-X. *et al.* Rapid Identification of Multiple Bacteria on a Microfluidic Chip. *Chinese Journal of Analytical Chemistry* **42**, 791-798 (2014).
104 Brouzes, E. *et al.* Droplet microfluidic technology for single-cell high-throughput screening. *Proceedings of the National Academy of Sciences* **106**, 14195-14200 (2009).
105 Love, J. C., Ronan, J. L., Grotenbreg, G. M., van der Veen, A. G. & Ploegh, H. L. A microengraving method for rapid selection of single cells producing antigen-specific antibodies. *Nature biotechnology* **24**, 703-707 (2006).
106 Stringari, C. *et al.* Phasor approach to fluorescence lifetime microscopy distinguishes different metabolic states of germ cells in a live tissue. *Proceedings of the National Academy of Sciences*, doi:10.1073/pnas.1108161108 (2011).
107 Lunt, S. Y. & Vander Heiden, M. G. Aerobic glycolysis: meeting the metabolic requirements of cell proliferation. *Annual review of cell and developmental biology* **27**, 441-464 (2011).
108 Roger, V. L. *et al.* AHA Statistical Update
Heart Disease and Stroke Statistics—2012 Update
A Report From the American Heart Association. *Circulation* **125**, e2-e220 (2012).
109 Bruneau, B. G. The developmental genetics of congenital heart disease. *Nature* **451**, 943-948, doi:nature06801 [pii]
10.1038/nature06801 (2008).
110 Lipshultz, S. E. *et al.* The incidence of pediatric cardiomyopathy in two regions of the United States. *N Engl J Med* **348**, 1647-1655, doi:10.1056/NEJMoa021715
348/17/1647 [pii] (2003).
111 Lexchin, J. Drug withdrawals from the Canadian market for safety reasons, 1963-2004. *CMAJ* **172**, 765-767, doi:172/6/765 [pii]
10.1503/cmaj.045021 (2005).
112 Denning, C. & Anderson, D. Cardiomyocytes from human embryonic stem cells as predictors of cardiotoxicity. *Drug Discovery Today: Therapeutic Strategies* **5**, 223-232 (2008).
113 Mandenius, C. F. *et al.* Cardiotoxicity testing using pluripotent stem cell-derived human cardiomyocytes and state-of-the-art bioanalytics: a review. *J Appl Toxicol* **31**, 191-205, doi:10.1002/jat.1663.
114 Dick, E., Rajamohan, D., Ronksley, J. & Denning, C. Evaluating the utility of cardiomyocytes from human pluripotent stem cells for drug screening. *Biochem Soc Trans* **38**, 1037-1045, doi:BST0381037 [pii]
10.1042/BST0381037.
115 Faustino, R. S. *et al.* Decoded calreticulin-deficient embryonic stem cell transcriptome resolves latent cardiophenotype. *Stem Cells* **28**, 1281-1291, doi:10.1002/stem.447.
116 Otsuji, T. G. *et al.* Progressive maturation in contracting cardiomyocytes derived from human embryonic stem cells: Qualitative effects on electrophysiological responses to drugs. *Stem Cell Res* **4**, 201-213, doi:S1873-5061(10)00013-9 [pii]
10.1016/j.scr.2010.01.002.
117 Yazawa, M. *et al.* Using induced pluripotent stem cells to investigate cardiac phenotypes in Timothy syndrome. *Nature* **471**, 230-234, doi:nature09855 [pii]
10.1038/nature09855.
118 Lahti, A. L. *et al.* Model for long QT syndrome type 2 using human iPS cells demonstrates arrhythmogenic characteristics in cell culture. *Dis Model Mech* **5**, 220-230, doi:dmm.008409 [pii]
10.1242/dmm.008409.
119 Itzhaki, I. *et al.* Modelling the long QT syndrome with induced pluripotent stem cells. *Nature* **471**, 225-229, doi:nature09747 [pii]
10.1038/nature09747.
120 Jung, C. B. *et al.* Dantrolene rescues arrhythmogenic RYR2 defect in a patient-specific stem cell model of catecholaminergic polymorphic ventricular tachycardia. *EMBO Mol Med* **4**, 180-191, doi:10.1002/emmm.201100194.
121 Caspi, O. & Gepstein, L. Regenerating the heart using human embryonic stem cells--from cell to bedside. *Isr Med Assoc J* **8**, 208-214 (2006).

122 Liu, J. *et al.* Generation, Characterization, and Potential Therapeutic Applications of Cardiomyocytes from Various Stem Cells. *Stem Cells Dev*, doi:10.1089/scd.2012.0031.
123 Vidarsson, H., Hyllner, J. & Sartipy, P. Differentiation of human embryonic stem cells to cardiomyocytes for in vitro and in vivo applications. *Stem Cell Rev* **6**, 108-120, doi:10.1007/s12015-010-9113-x.
124 Xu, C., Police, S., Rao, N. & Carpenter, M. K. Characterization and enrichment of cardiomyocytes derived from human embryonic stem cells. *Circ Res* **91**, 501-508 (2002).
125 Rose, R. A. *et al.* Bone marrow-derived mesenchymal stromal cells express cardiac-specific markers, retain the stromal phenotype, and do not become functional cardiomyocytes in vitro. *Stem Cells* **26**, 2884-2892, doi:2008-0329 [pii]
10.1634/stemcells.2008-0329 (2008).
126 Rangappa, S., Fen, C., Lee, E. H., Bongso, A. & Sim, E. K. Transformation of adult mesenchymal stem cells isolated from the fatty tissue into cardiomyocytes. *Ann Thorac Surg* **75**, 775-779 (2003).
127 Heubach, J. F. *et al.* Electrophysiological properties of human mesenchymal stem cells. *J Physiol* **554**, 659-672, doi:10.1113/jphysiol.2003.055806
jphysiol.2003.055806 [pii] (2004).
128 Fukuda, K. Reprogramming of bone marrow mesenchymal stem cells into cardiomyocytes. *C R Biol* **325**, 1027-1038 (2002).
129 Sachinidis, A. *et al.* Cardiac specific differentiation of mouse embryonic stem cells. *Cardiovasc Res* **58**, 278-291, doi:S0008636303002487 [pii] (2003).
130 Smith, A. G. Embryo-derived stem cells: of mice and men. *Annu Rev Cell Dev Biol* **17**, 435-462, doi:10.1146/annurev.cellbio.17.1.435
17/1/435 [pii] (2001).
131 Mummery, C. *et al.* Cardiomyocyte differentiation of mouse and human embryonic stem cells. *J Anat* **200**, 233-242 (2002).
132 Boheler, K. R. *et al.* Differentiation of pluripotent embryonic stem cells into cardiomyocytes. *Circ Res* **91**, 189-201 (2002).
133 Mummery, C. L. *et al.* Differentiation of human embryonic stem cells and induced pluripotent stem cells to cardiomyocytes: a methods overview. *Circ Res* **111**, 344-358, doi:111/3/344 [pii]
10.1161/CIRCRESAHA.110.227512.
134 Jiang, J., Han, P., Zhang, Q., Zhao, J. & Ma, Y. Cardiac Differentiation of Human Pluripotent Stem Cells. *J Cell Mol Med*, doi:10.1111/j.1582-4934.2012.01528.x.
135 David, R. & Franz, W. M. From pluripotency to distinct cardiomyocyte subtypes. *Physiology (Bethesda)* **27**, 119-129, doi:27/3/119 [pii]
10.1152/physiol.00044.2011.
136 Habib, M., Caspi, O. & Gepstein, L. Human embryonic stem cells for cardiomyogenesis. *J Mol Cell Cardiol* **45**, 462-474, doi:S0022-2828(08)00574-9 [pii]
10.1016/j.yjmcc.2008.08.008 (2008).
137 Blazeski, A. *et al.* Electrophysiological and contractile function of cardiomyocytes derived from human embryonic stem cells. *Prog Biophys Mol Biol*, doi:S0079-6107(12)00065-X [pii]
10.1016/j.pbiomolbio.2012.07.012.
138 Barile, L. *et al.* Cardiac stem cells: isolation, expansion and experimental use for myocardial regeneration. *Nat Clin Pract Cardiovasc Med* **4 Suppl 1**, S9-S14, doi:ncpcardio0738 [pii]
10.1038/ncpcardio0738 (2007).
139 Gherghiceanu, M. *et al.* Cardiomyocytes derived from human embryonic and induced pluripotent stem cells: comparative ultrastructure. *J Cell Mol Med* **15**, 2539-2551, doi:10.1111/j.1582-4934.2011.01417.x.
140 Sartiani, L., Bochet, P., Cerbai, E., Mugelli, A. & Fischmeister, R. Functional expression of the hyperpolarization-activated, non-selective cation current If in immortalized HL-1 cardiomyocytes. *The Journal of Physiology* **545**, 81-92, doi:10.1113/jphysiol.2002.021535 (2002).
141 Kim, C. *et al.* Non-Cardiomyocytes Influence the Electrophysiological Maturation of Human Embryonic Stem Cell-Derived Cardiomyocytes During Differentiation. *Stem Cells and Development* **19**, 783-795, doi:Doi 10.1089/Scd.2009.0349 (2010).
142 Bauwens, C. L. *et al.* Control of human embryonic stem cell colony and aggregate size heterogeneity influences differentiation trajectories. *Stem Cells* **26**, 2300-2310, doi:2008-0183 [pii]
10.1634/stemcells.2008-0183 (2008).

143 McDevitt, T. C., Laflamme, M. A. & Murry, C. E. Proliferation of cardiomyocytes derived from human embryonic stem cells is mediated via the IGF/PI 3-kinase/Akt signaling pathway. *J Mol Cell Cardiol* **39**, 865-873, doi:S0022-2828(05)00287-7 [pii]
10.1016/j.yjmcc.2005.09.007 (2005).
144 Mummery, C. *et al.* Differentiation of human embryonic stem cells to cardiomyocytes: role of coculture with visceral endoderm-like cells. *Circulation* **107**, 2733-2740, doi:10.1161/01.CIR.0000068356.38592.68
01.CIR.0000068356.38592.68 [pii] (2003).
145 Fijnvandraat, A. C. *et al.* Cardiomyocytes derived from embryonic stem cells resemble cardiomyocytes of the embryonic heart tube. *Cardiovasc Res* **58**, 399-409, doi:S0008636303002827 [pii] (2003).
146 Li, R. A. *et al.* Absence of Transverse Tubules Contributes to Non-Uniform Ca(2+) Wavefronts in Mouse and Human Embryonic Stem Cell-Derived Cardiomyocytes. *Stem Cells and Development* **18**, 1493-1500, doi:Doi 10.1089/Scd.2009.0052 (2009).
147 Smolich, J. J. Ultrastructural and functional features of the developing mammalian heart: a brief overview. *Reprod Fertil Dev* **7**, 451-461 (1995).
148 Gepstein, L. *et al.* Assessment of the ultrastructural and proliferative properties of human embryonic stem cell-derived cardiomyocytes. *American Journal of Physiology-Heart and Circulatory Physiology* **285**, H2355-H2363, doi:Doi 10.1152/Ajpheart.00020.2003 (2003).
149 Binah, O. *et al.* Functional and developmental properties of human embryonic stem cells-derived cardiomyocytes. *J Electrocardiol* **40**, S192-196, doi:S0022-0736(07)00651-6 [pii]
10.1016/j.jelectrocard.2007.05.035 (2007).
150 Dolnikov, K. *et al.* Functional Properties of Human Embryonic Stem Cell Derived Cardiomyocytes: Intracellular Ca2+ Handling and the Role of Sarcoplasmic Reticulum in the Contraction. *Stem Cells* **24**, 236-245 (2006).
151 Fu, J. D. *et al.* Crucial role of the sarcoplasmic reticulum in the developmental regulation of Ca2+ transients and contraction in cardiomyocytes derived from embryonic stem cells. *FASEB J* **20**, 181-183, doi:05-4501fje [pii]
10.1096/fj.05-4501fje (2006).
152 Itzhaki, I., Schiller, J., Beyar, R., Satin, J. & Gepstein, L. Calcium handling in embryonic stem cell-derived cardiac myocytes: of mice and men. *Ann N Y Acad Sci* **1080**, 207-215, doi:1080/1/207 [pii]
10.1196/annals.1380.017 (2006).
153 Cui, L., Johkura, K., Takei, S., Ogiwara, N. & Sasaki, K. Structural differentiation, proliferation, and association of human embryonic stem cell-derived cardiomyocytes in vitro and in their extracardiac tissues. *J Struct Biol* **158**, 307-317, doi:S1047-8477(06)00380-7 [pii]
10.1016/j.jsb.2006.11.009 (2007).
154 Erokhina, I. L., Semenova, E. G. & Emel'ianova, O. I. [Human fetal ventricular cardiomyocytes in vitro: proliferation and differentiation]. *Tsitologiia* **47**, 200-206 (2005).
155 Horigome, H. *et al.* Magnetocardiographic determination of the developmental changes in PQ, QRS and QT intervals in the foetus. *Acta Paediatr* **89**, 64-67 (2000).
156 Porrello, E. R. *et al.* Transient Regenerative Potential of the Neonatal Mouse Heart. *Science* **331**, 1078-1080, doi:Doi 10.1126/Science.1200708 (2011).
157 Bergmann, O. *et al.* Evidence for Cardiomyocyte Renewal in Humans. *Science* **324**, 98-102, doi:10.1126/science.1164680 (2009).
158 Cowan, C. A. *et al.* Derivation of embryonic stem-cell lines from human blastocysts. *N Engl J Med* **350**, 1353-1356, doi:10.1056/NEJMsr040330
NEJMsr040330 [pii] (2004).
159 Horio, T. *et al.* Inhibitory regulation of hypertrophy by endogenous atrial natriuretic peptide in cultured cardiac myocytes. *Hypertension* **35**, 19-24 (2000).
160 Holtwick, R. *et al.* Pressure-independent cardiac hypertrophy in mice with cardiomyocyte-restricted inactivation of the atrial natriuretic peptide receptor guanylyl cyclase-A. *Journal of Clinical Investigation* **111**, 1399-1407, doi:Doi 10.1172/Jci200317061 (2003).
161 Tanaka, T. *et al.* In vitro pharmacologic testing using human induced pluripotent stem cell-derived cardiomyocytes. *Biochem Bioph Res Co* **385**, 497-502, doi:Doi 10.1016/J.Bbrc.2009.05.073 (2009).
162 Kehat, I. *et al.* Human embryonic stem cells can differentiate into myocytes with structural and functional properties of cardiomyocytes. *Journal of Clinical Investigation* **108**, 407-414 (2001).
163 Cao, F. *et al.* Transcriptional and functional profiling of human embryonic stem cell-derived cardiomyocytes. *Plos One* **3**, e3474, doi:10.1371/journal.pone.0003474 (2008).

164 Synnergren, J. *et al.* Cardiomyogenic gene expression profiling of differentiating human embryonic stem cells. *J Biotechnol* **134**, 162-170, doi:S0168-1656(07)01748-8 [pii]
10.1016/j.jbiotec.2007.11.011 (2008).
165 Synnergren, J. *et al.* Molecular signature of cardiomyocyte clusters derived from human embryonic stem cells. *Stem Cells* **26**, 1831-1840, doi:2007-1033 [pii]
10.1634/stemcells.2007-1033 (2008).
166 Synnergren, J. *et al.* Differentiating human embryonic stem cells express a unique housekeeping gene signature. *Stem Cells* **25**, 473-480, doi:25/2/473 [pii]
10.1634/stemcells.2006-0247 (2007).
167 Gupta, M. K. *et al.* Global transcriptional profiles of beating clusters derived from human induced pluripotent stem cells and embryonic stem cells are highly similar. *BMC Dev Biol* **10**, 98, doi:1471-213X-10-98 [pii]
10.1186/1471-213X-10-98.
168 Synnergren, J. *et al.* Transcriptional profiling of human embryonic stem cells differentiating to definitive and primitive endoderm and further toward the hepatic lineage. *Stem Cells Dev* **19**, 961-978, doi:10.1089/scd.2009.0220.
169 Tashiro, A., Masuda, T. & Segawa, I. Morphometric comparison of mitochondria and myofibrils of cardiomyocytes between hypertrophic and dilated cardiomyopathies. *Virchows Arch A Pathol Anat Histopathol* **416**, 473-478 (1990).
170 Barth, E., Stammler, G., Speiser, B. & Schaper, J. Ultrastructural quantitation of mitochondria and myofilaments in cardiac muscle from 10 different animal species including man. *J Mol Cell Cardiol* **24**, 669-681, doi:0022-2828(92)93381-S [pii] (1992).
171 Porter, G. A., Jr. *et al.* Bioenergetics, mitochondria, and cardiac myocyte differentiation. *Prog Pediatr Cardiol* **31**, 75-81, doi:10.1016/j.ppedcard.2011.02.002.
172 Kehat, I. *et al.* Human embryonic stem cells can differentiate into myocytes with structural and functional properties of cardiomyocytes. *J Clin Invest* **108**, 407-414, doi:10.1172/JCI12131 (2001).
173 Awasthi, S. *et al.* Label-free identification and characterization of human pluripotent stem cell-derived cardiomyocytes using second harmonic generation (SHG) microscopy. *J Biophotonics* **5**, 57-66, doi:10.1002/jbio.201100077.
174 Giordano, F. J. Oxygen, oxidative stress, hypoxia, and heart failure. *J Clin Invest* **115**, 500-508, doi:10.1172/JCI24408 (2005).
175 Harris, D. A. & Das, A. M. Control of mitochondrial ATP synthesis in the heart. *Biochem J* **280 ( Pt 3)**, 561-573 (1991).
176 Lopaschuk, G. D., Collins-Nakai, R. L. & Itoi, T. Developmental changes in energy substrate use by the heart. *Cardiovasc Res* **26**, 1172-1180 (1992).
177 Lopaschuk, G. & Jaswal, J. Energy metabolic phenotype of the cardiomyocyte during development, differentiation and postnatal maturation. *Journal of Cardiovascular Pharmacology* **56**, 130-140, doi:10.1097/FJC.0b013e3181e74a14 (2010).
178 Rana, P., Anson, B., Engle, S. & Will, Y. Characterization of Human Induced Pluripotent Stem Cell Derived Cardiomyocytes: Bioenergetics and Utilization in Safety Screening. *Toxicol Sci*, doi:kfs233 [pii]
10.1093/toxsci/kfs233.
179 St John, J. C. *et al.* The expression of mitochondrial DNA transcription factors during early cardiomyocyte in vitro differentiation from human embryonic stem cells. *Cloning Stem Cells* **7**, 141-153, doi:10.1089/clo.2005.7.141 (2005).
180 Chung, S. *et al.* Mitochondrial oxidative metabolism is required for the cardiac differentiation of stem cells. *Nat Clin Pract Cardiovasc Med* **4 Suppl 1**, S60-67, doi:ncpcardio0766 [pii]
10.1038/ncpcardio0766 (2007).
181 Bistola, V. *et al.* Long-term primary cultures of human adult atrial cardiac myocytes: cell viability, structural properties and BNP secretion in vitro. *Int J Cardiol* **131**, 113-122, doi:S0167-5273(07)01946-8 [pii]
10.1016/j.ijcard.2007.10.058 (2008).
182 Mitcheson, J. S., Hancox, J. C. & Levi, A. J. Cultured adult cardiac myocytes: future applications, culture methods, morphological and electrophysiological properties. *Cardiovasc Res* **39**, 280-300, doi:S000863639800128X [pii] (1998).

183 Cohen, J. D. *et al.* Use of human stem cell derived cardiomyocytes to examine sunitinib mediated cardiotoxicity and electrophysiological alterations. *Toxicol Appl Pharmacol* **257**, 74-83, doi:S0041-008X(11)00334-6 [pii]
10.1016/j.taap.2011.08.020.
184 Simunek, T. *et al.* Anthracycline-induced cardiotoxicity: overview of studies examining the roles of oxidative stress and free cellular iron. *Pharmacol Rep* **61**, 154-171 (2009).
185 Andersson, H. *et al.* Assaying cardiac biomarkers for toxicity testing using biosensing and cardiomyocytes derived from human embryonic stem cells. *J Biotechnol* **150**, 175-181, doi:S0168-1656(10)00306-8 [pii]
10.1016/j.jbiotec.2010.06.023.
186 Shinozawa, T., Furukawa, H., Sato, E. & Takami, K. A Novel Purification Method of Murine Embryonic Stem Cell- and Human-Induced Pluripotent Stem Cell-Derived Cardiomyocytes by Simple Manual Dissociation. *J Biomol Screen*, doi:1087057111434145 [pii]
10.1177/1087057111434145.
187 Sepac, A. *et al.* Isoflurane preconditioning elicits competent endogenous mechanisms of protection from oxidative stress in cardiomyocytes derived from human embryonic stem cells. *Anesthesiology* **113**, 906-916, doi:10.1097/ALN.0b013e3181eff6b7.
188 Kim, J. H. *et al.* Isoflurane decreases death of human embryonic stem cell-derived, transcriptional marker Nkx2.5(+) cardiac progenitor cells. *Acta Anaesthesiol Scand* **55**, 1124-1131, doi:10.1111/j.1399-6576.2011.02509.x.
189 Ferdinandy, P., Schulz, R. & Baxter, G. F. Interaction of cardiovascular risk factors with myocardial ischemia/reperfusion injury, preconditioning, and postconditioning. *Pharmacol Rev* **59**, 418-458, doi:pr.107.06002 [pii]
10.1124/pr.107.06002 (2007).
190 Sedmera, D., Kucera, P. & Raddatz, E. Developmental changes in cardiac recovery from anoxia-reoxygenation. *Am J Physiol Regul Integr Comp Physiol* **283**, R379-388, doi:10.1152/ajpregu.00534.2001 (2002).
191 Kang, P. M., Haunstetter, A., Aoki, H., Usheva, A. & Izumo, S. Morphological and molecular characterization of adult cardiomyocyte apoptosis during hypoxia and reoxygenation. *Circ Res* **87**, 118-125 (2000).
192 Norstrom, A. *et al.* Molecular and pharmacological properties of human embryonic stem cell-derived cardiomyocytes. *Exp Biol Med (Maywood)* **231**, 1753-1762, doi:231/11/1753 [pii] (2006).
193 Brito-Martins, M., Harding, S. E. & Ali, N. N. beta(1)- and beta(2)-adrenoceptor responses in cardiomyocytes derived from human embryonic stem cells: comparison with failing and non-failing adult human heart. *Br J Pharmacol* **153**, 751-759, doi:0707619 [pii]
10.1038/sj.bjp.0707619 (2008).
194 Mehta, A. *et al.* Pharmacological response of human cardiomyocytes derived from virus-free induced pluripotent stem cells. *Cardiovasc Res* **91**, 577-586, doi:cvr132 [pii]
10.1093/cvr/cvr132.
195 Reppel, M., Boettinger, C. & Hescheler, J. Beta-adrenergic and muscarinic modulation of human embryonic stem cell-derived cardiomyocytes. *Cell Physiol Biochem* **14**, 187-196, doi:10.1159/000080326
80326 [pii] (2004).
196 Zwi, L. *et al.* Cardiomyocyte differentiation of human induced pluripotent stem cells. *Circulation* **120**, 1513-1523, doi:CIRCULATIONAHA.109.868885 [pii]
10.1161/CIRCULATIONAHA.109.868885 (2009).
197 Zwi, L. *et al.* Cardiomyocyte Differentiation of Human Induced Pluripotent Stem Cells. *Human Gene Therapy* **21**, 658-658 (2010).
198 Xue, T. *et al.* Functional integration of electrically active cardiac derivatives from genetically engineered human embryonic stem cells with quiescent recipient ventricular cardiomyocytes: insights into the development of cell-based pacemakers. *Circulation* **111**, 11-20, doi:01.CIR.0000151313.18547.A2 [pii]
10.1161/01.CIR.0000151313.18547.A2 (2005).
199 Satin, J. *et al.* Mechanism of spontaneous excitability in human embryonic stem cell derived cardiomyocytes. *J Physiol* **559**, 479-496, doi:10.1113/jphysiol.2004.068213
jphysiol.2004.068213 [pii] (2004).
200 Germanguz, I. *et al.* Molecular characterization and functional properties of cardiomyocytes derived from human inducible pluripotent stem cells. *J Cell Mol Med* **15**, 38-51, doi:JCMM996 [pii]
10.1111/j.1582-4934.2009.00996.x.

201 Pillekamp, F. *et al.* Contractile Properties of Early Human Embryonic Stem Cell-Derived Cardiomyocytes: Beta-Adrenergic Stimulation Induces Positive Chronotropy and Lusitropy but Not Inotropy. *Stem Cells Dev*, doi:10.1089/scd.2011.0312.
202 Burridge, P. W. *et al.* A Universal System for Highly Efficient Cardiac Differentiation of Human Induced Pluripotent Stem Cells That Eliminates Interline Variability. *Plos One* **6**, doi:ARTN e18293
DOI 10.1371/journal.pone.0018293 (2011).
203 Xu, R. H. *et al.* BMP4 initiates human embryonic stem cell differentiation to trophoblast. *Nat Biotechnol* **20**, 1261-1264, doi:10.1038/nbt761
nbt761 [pii] (2002).
204 Braam, S. R. *et al.* Prediction of drug-induced cardiotoxicity using human embryonic stem cell-derived cardiomyocytes. *Stem Cell Res* **4**, 107-116, doi:S1873-5061(09)00138-X [pii]
10.1016/j.scr.2009.11.004.
205 Wang, K. *et al.* Biophysical properties of slow potassium channels in human embryonic stem cell derived cardiomyocytes implicate subunit stoichiometry. *J Physiol* **589**, 6093-6104, doi:jphysiol.2011.220863 [pii]
10.1113/jphysiol.2011.220863.
206 Moretti, A. *et al.* Patient-specific induced pluripotent stem-cell models for long-QT syndrome. *N Engl J Med* **363**, 1397-1409, doi:NEJMoa0908679 [pii]
10.1056/NEJMoa0908679.
207 Bilic, J. & Izpisua Belmonte, J. C. Concise review: Induced pluripotent stem cells versus embryonic stem cells: close enough or yet too far apart? *Stem Cells* **30**, 33-41, doi:10.1002/stem.700.
208 He, J. Q., Ma, Y., Lee, Y., Thomson, J. A. & Kamp, T. J. Human embryonic stem cells develop into multiple types of cardiac myocytes: action potential characterization. *Circ Res* **93**, 32-39, doi:10.1161/01.RES.0000080317.92718.99
01.RES.0000080317.92718.99 [pii] (2003).
209 Zhu, W. Z. *et al.* Neuregulin/ErbB signaling regulates cardiac subtype specification in differentiating human embryonic stem cells. *Circ Res* **107**, 776-786, doi:CIRCRESAHA.110.223917 [pii]
10.1161/CIRCRESAHA.110.223917.
210 Moore, J. C. *et al.* Distinct cardiogenic preferences of two human embryonic stem cell (hESC) lines are imprinted in their proteomes in the pluripotent state. *Biochem Biophys Res Commun* **372**, 553-558, doi:S0006-291X(08)00969-8 [pii]
10.1016/j.bbrc.2008.05.076 (2008).
211 Pekkanen-Mattila, M. *et al.* Human embryonic stem cell-derived cardiomyocytes: demonstration of a portion of cardiac cells with fairly mature electrical phenotype. *Exp Biol Med (Maywood)* **235**, 522-530, doi:235/4/522 [pii]
10.1258/ebm.2010.009345.
212 Drouin, E., Lande, G. & Charpentier, F. Amiodarone reduces transmural heterogeneity of repolarization in the human heart. *J Am Coll Cardiol* **32**, 1063-1067, doi:S0735-1097(98)00330-1 [pii] (1998).
213 Yanagi, K. *et al.* Hyperpolarization-activated cyclic nucleotide-gated channels and T-type calcium channels confer automaticity of embryonic stem cell-derived cardiomyocytes. *Stem Cells* **25**, 2712-2719, doi:2006-0388 [pii]
10.1634/stemcells.2006-0388 (2007).
214 Pekkanen-Mattila, M. *et al.* The effect of human and mouse fibroblast feeder cells on cardiac differentiation of human pluripotent stem cells. *Stem Cells Int* **2012**, 875059, doi:10.1155/2012/875059.
215 Zhang, Q. *et al.* Direct differentiation of atrial and ventricular myocytes from human embryonic stem cells by alternating retinoid signals. *Cell Res* **21**, 579-587, doi:cr2010163 [pii]
10.1038/cr.2010.163.
216 Ma, J. *et al.* High purity human-induced pluripotent stem cell-derived cardiomyocytes: electrophysiological properties of action potentials and ionic currents. *Am J Physiol Heart Circ Physiol* **301**, H2006-2017, doi:ajpheart.00694.2011 [pii]
10.1152/ajpheart.00694.2011.
217 Veldkamp, M. W. *et al.* Norepinephrine induces action potential prolongation and early afterdepolarizations in ventricular myocytes isolated from human end-stage failing hearts. *Eur Heart J* **22**, 955-963, doi:10.1053/euhj.2000.2499
S0195668X00924990 [pii] (2001).

218 Pekkanen-Mattila, M. *et al.* Substantial variation in the cardiac differentiation of human embryonic stem cell lines derived and propagated under the same conditions--a comparison of multiple cell lines. *Ann Med* **41**, 360-370, doi:908063463 [pii]
10.1080/07853890802609542 (2009).
219 Fu, J. D. *et al.* Na+/Ca2+ exchanger is a determinant of excitation-contraction coupling in human embryonic stem cell-derived ventricular cardiomyocytes. *Stem Cells Dev* **19**, 773-782, doi:10.1089/scd.2009.0184.
220 Zahanich, I. *et al.* Rhythmic beating of stem cell-derived cardiac cells requires dynamic coupling of electrophysiology and Ca cycling. *J Mol Cell Cardiol* **50**, 66-76, doi:S0022-2828(10)00371-8 [pii]
10.1016/j.yjmcc.2010.09.018.
221 Caspi, O. *et al.* In vitro electrophysiological drug testing using human embryonic stem cell derived cardiomyocytes. *Stem Cells Dev* **18**, 161-172, doi:10.1089/scd.2007.0280 (2009).
222 Tanaka, T. *et al.* In vitro pharmacologic testing using human induced pluripotent stem cell-derived cardiomyocytes. *Biochem Biophys Res Commun* **385**, 497-502, doi:S0006-291X(09)01011-0 [pii]
10.1016/j.bbrc.2009.05.073 (2009).
223 Gorelik, J. *et al.* Embryonic stem cell-derived cardiomyocytes as a model to study fetal arrhythmia related to maternal disease. *Journal of Cellular and Molecular Medicine* **13**, 3730-3741, doi:Doi 10.1111/J.1582-4934.2009.00741.X (2009).
224 Bers, D. M. Cardiac excitation-contraction coupling. *Nature* **415**, 198-205, doi:10.1038/415198a
415198a [pii] (2002).
225 Satin, J. *et al.* Calcium handling in human embryonic stem cell-derived cardiomyocytes. *Stem Cells* **26**, 1961-1972, doi:2007-0591 [pii]
10.1634/stemcells.2007-0591 (2008).
226 Lee, Y. K. *et al.* Calcium homeostasis in human induced pluripotent stem cell-derived cardiomyocytes. *Stem Cell Rev* **7**, 976-986, doi:10.1007/s12015-011-9273-3.
227 Liu, J. *et al.* Facilitated maturation of Ca2+ handling properties of human embryonic stem cell-derived cardiomyocytes by calsequestrin expression. *Am J Physiol Cell Physiol* **297**, C152-159, doi:00060.2009 [pii]
10.1152/ajpcell.00060.2009 (2009).
228 Itzhaki, I. *et al.* Calcium handling in human induced pluripotent stem cell derived cardiomyocytes. *Plos One* **6**, e18037, doi:10.1371/journal.pone.0018037.
229 Dolnikov, K. *et al.* Functional properties of human embryonic stem cell-derived cardiomyocytes. *Ann N Y Acad Sci* **1047**, 66-75, doi:1047/1/66 [pii]
10.1196/annals.1341.006 (2005).
230 Kang, J., Chen, X., Ji, J., Lei, Q. & Rampe, D. Ca2+ Channel Activators Reveal Differential L-Type Ca2+ Channel Pharmacology between Native and Stem Cell-Derived Cardiomyocytes. *The journal of Pharmacology* **341**, 510-517 (2012).
231 Zhu, W. Z., Santana, L. F. & Laflamme, M. A. Local control of excitation-contraction coupling in human embryonic stem cell-derived cardiomyocytes. *Plos One* **4**, e5407, doi:10.1371/journal.pone.0005407 (2009).
232 Xi, J. *et al.* Comparison of contractile behavior of native murine ventricular tissue and cardiomyocytes derived from embryonic or induced pluripotent stem cells. *FASEB J* **24**, 2739-2751, doi:fj.09-145177 [pii]
10.1096/fj.09-145177.
233 Mandel, Y. *et al.* Human embryonic and induced pluripotent stem cell-derived cardiomyocytes exhibit beat rate variability and power-law behavior. *Circulation* **125**, 883-893, doi:CIRCULATIONAHA.111.045146 [pii]
10.1161/CIRCULATIONAHA.111.045146.
234 Matsa, E. & Denning, C. In Vitro Uses of Human Pluripotent Stem Cell-Derived Cardiomyocytes. *J Cardiovasc Transl Res*, doi:10.1007/s12265-012-9376-5.
235 Lieu, D. K. *et al.* Absence of transverse tubules contributes to non-uniform Ca(2+) wavefronts in mouse and human embryonic stem cell-derived cardiomyocytes. *Stem Cells Dev* **18**, 1493-1500, doi:10.1089/scd.2009.0052 (2009).
236 Roderick, H. L. & Bootman, M. D. Pacemaking, arrhythmias, inotropy and hypertrophy: the many possible facets of IP3 signalling in cardiac myocytes. *J Physiol* **581**, 883-884, doi:jphysiol.2007.133819 [pii]
10.1113/jphysiol.2007.133819 (2007).

237 Nakayama, H. *et al.* The IP3 receptor regulates cardiac hypertrophy in response to select stimuli. *Circ Res* **107**, 659-666, doi:CIRCRESAHA.110.220038 [pii]
10.1161/CIRCRESAHA.110.220038.
238 Hund, T. J., Ziman, A. P., Lederer, W. J. & Mohler, P. J. The cardiac IP3 receptor: uncovering the role of "the other" calcium-release channel. *J Mol Cell Cardiol* **45**, 159-161, doi:S0022-2828(08)00498-7 [pii]
10.1016/j.yjmcc.2008.06.001 (2008).
239 Liu, J., Fu, J. D., Siu, C. W. & Li, R. A. Functional sarcoplasmic reticulum for calcium handling of human embryonic stem cell-derived cardiomyocytes: insights for driven maturation. *Stem Cells* **25**, 3038-3044, doi:2007-0549 [pii]
10.1634/stemcells.2007-0549 (2007).
240 Lee, Y. K. *et al.* Triiodothyronine promotes cardiac differentiation and maturation of embryonic stem cells via the classical genomic pathway. *Mol Endocrinol* **24**, 1728-1736, doi:me.2010-0032 [pii]
10.1210/me.2010-0032.
241 Ng, K. M. *et al.* Exogenous expression of HIF-1 alpha promotes cardiac differentiation of embryonic stem cells. *J Mol Cell Cardiol* **48**, 1129-1137, doi:S0022-2828(10)00028-3 [pii]
10.1016/j.yjmcc.2010.01.015.
242 Bers, D. M. *Excitation-Contraction Coupling and Cardiac Contractile Force*. 2 edn, (Kluwer Academic Publishers, 2001).
243 Chaudhary, K. W. *et al.* Embryonic stem cells in predictive cardiotoxicity: laser capture microscopy enables assay development. *Toxicol Sci* **90**, 149-158, doi:kfj078 [pii]
10.1093/toxsci/kfj078 (2006).
244 Luo, W. *et al.* Targeted ablation of the phospholamban gene is associated with markedly enhanced myocardial contractility and loss of beta-agonist stimulation. *Circ Res* **75**, 401-409 (1994).
245 MacLennan, D. H. & Kranias, E. G. Phospholamban: a crucial regulator of cardiac contractility. *Nat Rev Mol Cell Biol* **4**, 566-577, doi:10.1038/nrm1151
nrm1151 [pii] (2003).
246 Gyorke, I., Hester, N., Jones, L. R. & Gyorke, S. The role of calsequestrin, triadin, and junctin in conferring cardiac ryanodine receptor responsiveness to luminal calcium. *Biophys J* **86**, 2121-2128, doi:S0006-3495(04)74271-X [pii]
10.1016/S0006-3495(04)74271-X (2004).
247 Pegram, M. & Ngo, D. Application and potential limitations of animal models utilized in the development of trastuzumab (Herceptin((R))): A case study. *Adv Drug Deliver Rev* **58**, 723-734, doi:Doi 10.1016/J.Addr.2006.05.003 (2006).
248 Carroll, J. *UPDATED: Deadly tox threat kills Bristol-Myers' $2.5B hep C prospect*

*Read more: UPDATED: Deadly tox threat kills Bristol-Myers' $2.5B hep C prospect - FierceBiotech* http://www.fiercebiotech.com/story/deadly-tox-threat-kills-bristol-myers-once-brilliant-25b-hep-c-prospect/2012-08-23 - ixzz2b5hRImAg
*Subscribe at FierceBiotech*, <http://www.fiercebiotech.com/story/deadly-tox-threat-kills-bristol-myers-once-brilliant-25b-hep-c-prospect/2012-08-23> (2012).
249 Krumholz, H. M., Ross, J. S., Presler, A. H. & Egilman, D. S. What have we learnt from Vioxx? *BMJ: British Medical Journal* **334**, 120 (2007).
250 Karakikes, I. *et al.* Small molecule-mediated directed differentiation of human embryonic stem cells toward ventricular cardiomyocytes. *Stem cells translational medicine* **3**, 18-31 (2014).
251 Josowitz, R. *et al.* Identification and Purification of Human Induced Pluripotent Stem Cell-Derived Atrial-Like Cardiomyocytes Based on Sarcolipin Expression. *Plos One* **9**, e101316 (2014).
252 Ma, J. *et al.* High purity human-induced pluripotent stem cell-derived cardiomyocytes: electrophysiological properties of action potentials and ionic currents. *American Journal of Physiology-Heart and Circulatory Physiology* **301**, H2006-H2017 (2011).
253 Lahti, A. L. *et al.* Model for long QT syndrome type 2 using human iPS cells demonstrates arrhythmogenic characteristics in cell culture. *Disease models & mechanisms* **5**, 220-230 (2012).
254 Moretti, A. *et al.* Patient-specific induced pluripotent stem-cell models for long-QT syndrome. *New England Journal of Medicine* **363**, 1397-1409 (2010).
255 Nguyen, D. C. *et al.* Microscale generation of cardiospheres promotes robust enrichment of cardiomyocytes derived from human pluripotent stem cells. *Stem cell reports* **3**, 260-268 (2014).

256 Beauchamp, P. *et al.* Development and characterization of a scaffold-free 3D spheroid model of iPSC-derived human cardiomyocytes. *Tissue Engineering* (2015).
257 Huss, J. M. & Kelly, D. P. Mitochondrial energy metabolism in heart failure: a question of balance. *The Journal of clinical investigation* **115**, 547-555 (2005).
258 Bers, D. *Excitation-contraction coupling and cardiac contractile force*. Vol. 237 (Springer Science & Business Media, 2001).
259 Peterson, L. R. *et al.* Effect of obesity and insulin resistance on myocardial substrate metabolism and efficiency in young women. *Circulation* **109**, 2191-2196 (2004).
260 Wu, M. *et al.* Multiparameter metabolic analysis reveals a close link between attenuated mitochondrial bioenergetic function and enhanced glycolysis dependency in human tumor cells. *American Journal of Physiology-Cell Physiology* **292**, C125-C136 (2007).
261 Kim, J. B. & Spiegelman, B. M. ADD1/SREBP1 promotes adipocyte differentiation and gene expression linked to fatty acid metabolism. *Genes & Development* **10**, 1096-1107 (1996).
262 Lu, H., Buchan, R. J. & Cook, S. A. MicroRNA-223 regulates Glut4 expression and cardiomyocyte glucose metabolism. *Cardiovasc Res* **86**, 410-420 (2010).
263 St. John, J. C. *et al.* The expression of mitochondrial DNA transcription factors during early cardiomyocyte in vitro differentiation from human embryonic stem cells. *Cloning and stem cells* **7**, 141-153 (2005).
264 Chen, K. *et al.* Caloric restriction mimetic 2-deoxyglucose antagonizes doxorubicin-induced cardiomyocyte death by multiple mechanisms. *Journal of Biological Chemistry* **286**, 21993-22006 (2011).
265 Stringari, C., Nourse, J. L., Flanagan, L. A. & Gratton, E. Phasor fluorescence lifetime microscopy of free and protein-bound NADH reveals neural stem cell differentiation potential. *Plos One* **7**, e48014 (2012).
266 Stringari, C. *et al.* Phasor approach to fluorescence lifetime microscopy distinguishes different metabolic states of germ cells in a live tissue. *Proceedings of the National Academy of Sciences* **108**, 13582-13587 (2011).
267 Stringari, C., Sierra, R., Donovan, P. J. & Gratton, E. Label-free separation of human embryonic stem cells and their differentiating progenies by phasor fluorescence lifetime microscopy. *Journal of biomedical optics* **17**, 0460121-04601211 (2012).
268 Lakowicz, J. R., Szmacinski, H., Nowaczyk, K. & Johnson, M. L. Fluorescence lifetime imaging of free and protein-bound NADH. *Proceedings of the National Academy of Sciences* **89**, 1271-1275 (1992).
269 Digman, M. A., Caiolfa, V. R., Zamai, M. & Gratton, E. The phasor approach to fluorescence lifetime imaging analysis. *Biophysical journal* **94**, L14-L16 (2008).
270 Kreitzer, F. R. *et al.* A robust method to derive functional neural crest cells from human pluripotent stem cells. *American journal of stem cells* **2**, 119 (2013).
271 Miyaoka, Y. *et al.* Isolation of single-base genome-edited human iPS cells without antibiotic selection. *Nature methods* **11**, 291-293 (2014).
272 Huebsch, N. *et al.* Automated Video-Based Analysis of Contractility and Calcium Flux in Human-Induced Pluripotent Stem-Derived Cardiomyocytes Cultured over Different Spatial Scales. *Tissue Engineering Part C: Methods* (2015).
273 Chen, T.-W. *et al.* Ultrasensitive fluorescent proteins for imaging neuronal activity. *Nature* **499**, 295-300 (2013).
274 Hockemeyer, D. *et al.* Genetic engineering of human pluripotent cells using TALE nucleases. *Nature biotechnology* **29**, 731-734 (2011).
275 Hosseinkhani, H., Hosseinkhani, M., Hattori, S., Matsuoka, R. & Kawaguchi, N. Micro and nano-scale in vitro 3D culture system for cardiac stem cells. *Journal of biomedical materials research Part A* **94**, 1-8 (2010).
276 Fischbach, C. *et al.* Engineering tumors with 3D scaffolds. *Nature methods* **4**, 855-860 (2007).
277 Baharvand, H., Azarnia, M., Parivar, K. & Ashtiani, S. K. The effect of extracellular matrix on embryonic stem cell-derived cardiomyocytes. *Journal of molecular and cellular cardiology* **38**, 495-503 (2005).
278 Kamakura, T. *et al.* Ultrastructural maturation of human-induced pluripotent stem cell-derived cardiomyocytes in a long-term culture. *Circulation Journal* **77**, 1307-1314 (2013).
279 Robertson, C., Tran, D. D. & George, S. C. Concise Review: Maturation Phases of Human Pluripotent Stem Cell-Derived Cardiomyocytes. *Stem Cells* **31**, 829-837 (2013).
280 Yang, X., Pabon, L. & Murry, C. E. Engineering Adolescence Maturation of Human Pluripotent Stem Cell-Derived Cardiomyocytes. *Circulation research* **114**, 511-523 (2014).
281 Misfeldt, A. M. *et al.* Endocardial cells are a distinct endothelial lineage derived from Flk1+ multipotent cardiovascular progenitors. *Developmental biology* **333**, 78-89 (2009).

282 Brutsaert, D. L. Cardiac endothelial-myocardial signaling: its role in cardiac growth, contractile performance, and rhythmicity. *Physiol Rev* **83**, 59-115, doi:10.1152/physrev.00017.2002 (2003).
283 Hsieh, P. C., Davis, M. E., Lisowski, L. K. & Lee, R. T. Endothelial-cardiomyocyte interactions in cardiac development and repair. *Annual review of physiology* **68**, 51 (2006).
284 Li, K., Rouleau, J., Andries, L. & Brutsaert, D. Effect of dysfunctional vascular endothelium on myocardial performance in isolated papillary muscles. *Circulation research* **72**, 768-777 (1993).
285 McClellan, G., Weisberg, A., Rose, D. & Winegrad, S. Endothelial cell storage and release of endothelin as a cardioregulatory mechanism. *Circulation research* **75**, 85-96 (1994).
286 Zhao, Y.-y. *et al.* Neuregulins promote survival and growth of cardiac myocytes Persistence of ErbB2 and ErbB4 expression in neonatal and adult ventricular myocytes. *Journal of Biological Chemistry* **273**, 10261-10269 (1998).
287 Narmoneva, D. A., Vukmirovic, R., Davis, M. E., Kamm, R. D. & Lee, R. T. Endothelial Cells Promote Cardiac Myocyte Survival and Spatial Reorganization Implications for Cardiac Regeneration. *Circulation* **110**, 962-968 (2004).
288 Zhang, M. & Shah, A. M. ROS signalling between endothelial cells and cardiac cells. *Cardiovascular research* **102**, 249-257 (2014).
289 Davis, M. E., Grumbach, I. M., Fukai, T., Cutchins, A. & Harrison, D. G. Shear stress regulates endothelial nitric-oxide synthase promoter activity through nuclear factor ŒʃB binding. *Journal of Biological Chemistry* **279**, 163-168 (2004).
290 Dimmeler, S. *et al.* Activation of nitric oxide synthase in endothelial cells by Akt-dependent phosphorylation. *Nature* **399**, 601-605 (1999).
291 Buga, G. M., Gold, M. E., Fukuto, J. M. & Ignarro, L. J. Shear stress-induced release of nitric oxide from endothelial cells grown on beads. *Hypertension* **17**, 187-193 (1991).
292 Mohan, P., Brutsaert, D. L., Paulus, W. J. & Sys, S. U. Myocardial contractile response to nitric oxide and cGMP. *Circulation* **93**, 1223-1229 (1996).
293 Paulus, W. J., Vantrimpont, P. J. & Shah, A. M. Paracrine coronary endothelial control of left ventricular function in humans. *Circulation* **92**, 2119-2126 (1995).
294 Kaye, D. M., Wiviott, S. D. & Kelly, R. A. Activation of Nitric Oxide Synthase (NOS3) by Mechanical Activity Alters Contractile Activity in a Ca< sup> 2+</sup>-Independent Manner in Cardiac Myocytes: Role of Troponin I Phosphorylation. *Biochem Bioph Res Co* **256**, 398-403 (1999).
295 Zhang, R., Zhao, J., Mandveno, A. & Potter, J. D. Cardiac troponin I phosphorylation increases the rate of cardiac muscle relaxation. *Circulation research* **76**, 1028-1035 (1995).
296 Prendergast, B. D., Sagach, V. F. & Shah, A. M. Basal release of nitric oxide augments the Frank-Starling response in the isolated heart. *Circulation* **96**, 1320-1329 (1997).
297 Petroff, M. G. *et al.* Endogenous nitric oxide mechanisms mediate the stretch dependence of Ca2+ release in cardiomyocytes. *Nat Cell Biol* **3**, 867-873, doi:10.1038/ncb1001-867 ncb1001-867 [pii] (2001).
298 Jaba, I. M. *et al.* NO triggers RGS4 degradation to coordinate angiogenesis and cardiomyocyte growth. *The Journal of clinical investigation* **123**, 1718-1731 (2013).
299 Zudaire, E., Gambardella, L., Kurcz, C. & Vermeren, S. A computational tool for quantitative analysis of vascular networks. *Plos One* **6**, e27385 (2011).
300 Swartz, M. A. & Fleury, M. E. Interstitial flow and its effects in soft tissues. *Annu. Rev. Biomed. Eng.* **9**, 229-256 (2007).